ฤทธิ์ต้านการสร้างหลอดเลือดใหม่และความเป็นพิษต่อเซลล์ของโรตินอยด์จากถอบแถบทะเล *Derris trifoliata* Lour.

นางสาวญาณิศา มิตรภาพ

วิทยานิพนธ์นี้เป็นส่วนหนึ่งของการศึกษาตามหลักสูตรปริญญาวิทยาศาสตรมหาบัณฑิต
สาขาวิชาเคมี ภาควิชาเคมี
คณะวิทยาศาสตร์ จุฬาลงกรณ์มหาวิทยาลัย
ปีการศึกษา 2560

ANTI-ANGIOGENIC AND CYTOTOXIC ACTIVITIES OF ROTENOIDS FROM *Derris trifoliata* Lour.

Miss Yanisa Mittraphab

A Thesis Submitted in Partial Fulfillment of the Requirements
for the Degree of Master of Science Program in Chemistry
Department of Chemistry
Faculty of Science
Chulalongkorn University
Academic Year 2017

Thesis Title	ANTI-ANGIOGENIC AND CYTOTOXIC ACTIVITIES OF ROTENOIDSFROM *Derris trifoliata* Lour.
By	Miss Yanisa Mittraphab
Field of Study	Chemistry
Thesis Advisor	Associate Professor Khanitha Pudhom, Ph.D.

Accepted by the Faculty of Science, Chulalongkorn University in Partial Fulfillment of the Requirements for the Master's Degree

.....Dean of the Faculty of Science

(Associate Professor Polkit Sangvanich, Ph.D.)

THESIS COMMITTEE

.....Chairman

(Associate Professor Vudhichai Parasuk, Ph.D.)

.....Thesis Advisor

(Associate Professor Khanitha Pudhom, Ph.D.)

.....Examiner

(Associate Professor Nattaya Ngamrojanavanich, Ph.D.)

.....External Examiner

(Assistant Professor Vachiraporn Ajavakom, Ph.D.)

ญาณิศา มิตรภาพ : ฤทธิ์ต้านการสร้างหลอดเลือดใหม่และความเป็นพิษต่อเซลล์ของโรตินอยด์จากถอบแถบทะเล *Derris trifoliata* Lour. (ANTI-ANGIOGENIC AND CYTOTOXIC ACTIVITIES OF ROTENOIDSFROM *Derris trifoliata* Lour.) อ.ที่ปรึกษาวิทยานิพนธ์หลัก: รศ. ดร.ขนิษฐา พุดหอม, 70 หน้า.

งานวิจัยนี้มีวัตถุประสงค์เพื่อแยกสารแมทตาบอไลท์ของต้นถอบแถบทะเล D. trifoliata และทดสอบความเป็นพิษต่อเซลล์และฤทธิ์ต้านการสร้างหลอดเลือดใหม่ จากการนำส่วนสกัดหยาบเอทิลแอซีเทตมาทำการแยกด้วยวิธีโครมาโทกราฟีต่างๆ พบโรตินอยด์ที่มีการรายงานมาแล้ว 8 ชนิด (1-2, 4-6, 11-12 and 15) เมื่อนำสารเหล่านี้มาทดสอบความเป็นพิษต่อเซลล์มะเร็ง 3 ชนิด คือ มะเร็งปากมดลูก, มะเร็งลำไส้ใหญ่, มะเร็งตับ และเซลล์ปกติ พบว่าสารประกอบทุกชนิดแสดงฤทธิ์ยับยั้งเซลล์มะเร็งลำไส้ใหญ่ โดยมีค่า IC_{50} อยู่ระหว่าง 0.12-11.21 μM ในขณะที่สารปะกอบทุกชนิดมีความเป็นพิษต่อเซลล์มะเร็งตับและมะเร็งปากมดลูกค่อนข้างต่ำหรือไม่มีฤทธิ์ อย่างไรก็ตาม 12a-hydroxyrotenone (11) สามารถยับยั้งการไมเกรทของเซลล์มะเร็งลำไส้ใหญ่ (ยับยั้งได้มากกว่า 90% ที่ความเข้มข้น 0.5 μM) เมื่อนำสารเหล่านี้มาทดสอบฤทธิ์ต้านการสร้างหลอดเลือดใหม่ พบว่า 12a-hydroxyrotenone (11) สามารถยับยั้งการสร้างหลอดเลือดใหม่ได้ดีมากทั้งในระดับ ex vivo และ in vitro ซึ่งเป็นผลมาจากการยับยั้งการเพิ่มจำนวน (proliferation) และยับยั้งการเปลี่ยนรูปเป็นหลอดเลือด (tube formation) แต่ไม่สามารถยับยั้งการไมเกรท (chemotactic migration) ของเซลล์เยื่อบุพนังหลอดเลือดได้ ดังนั้น 12a-hydroxyrotenone (11) อาจเป็นสารต้นแบบหรือสามารถนำไปใช้ประโยชน์ในทางโรคมะเร็งได้

ภาควิชา เคมี ลายมือชื่อนิสิต .....

สาขาวิชา เคมี ลายมือชื่อ อ.ที่ปรึกษาหลัก .....

ปีการศึกษา 2560

5771963023 : MAJOR CHEMISTRY
KEYWORDS: ROTENOID / DERRIS TRIFOLIATA / LEGUMINOSAE / CYTOTOXICITY / ANTI-ANGIOGENESIS / CANCER MIGRATION

YANISA MITTRAPHAB: ANTI-ANGIOGENIC AND CYTOTOXIC ACTIVITIES OF ROTENOIDSFROM *Derris trifoliata* Lour.. ADVISOR: ASSOC. PROF. KHANITHA PUDHOM, Ph.D., 70 pp.

This study aimed to isolate metabolites of *D. trifoliata* stem and to evaluate their cytotoxic and anti-angiogenic activities. Chromatographic fractionation of the EtOAc led to the isolation of eight known rotenoids (1-2, 4-6, 11-12 and 15). All compounds were first evaluated for their cytotoxicity against three cancer cell lines; human cervical carcinoma (CaSki), colon cancer (HCT-116), hepato carcinoma (Hep-G2) and normal human colon epithelial (CCD841) cells. All Compounds showed cytotoxicity against HCT-116 with IC_{50} ranging 0.12-11.21 μM, while they were weak or no activity against Hep-G2 and CaSKi cells. Moreover, it was found that 12a-hydroxyrotenone (11) potently inhibited migration of colon cancer HCT-116 cells (>90% inhibition at 0.5 μM). Further, all isolated compounds were evaluated for anti-angiogenic activity. Results indicated that 12a-hydorxyrotenone (11) displayed promising anti-angiogenic activity in both ex vivo and in vitro assays, as well as it mainly functions by suppression of endothelial cells (ECs) proliferation and tube formation, but did not show any significant effect on ECs migration. This is the first study providing the evidence that compound 11 has high potency on HCT-116 cancer growth and migration, as well as it is a potent anti-angiogenic agent. Thus, compound 11 may be suitable for use as a lead compound or for further development to overcome cancer metastasis.

Department: Chemistry Student's Signature .....
Field of Study: Chemistry Advisor's Signature .....
Academic Year: 2017

ACKNOWLEDGEMENTS

I would like to express my sincere appreciation to my advisor, Associate Professor Dr. Khanitha Pudhom, Department of Chemistry, Faculty of Science, Chulalongkorn University for her excellent instruction, her valuable guidance, which motivated me to pass through this course successfully.

In addition, many thanks to the Chairperson: Associate Professor Dr. Vudhichai Parasuk, Department of Chemistry, Faculty of Science, Chulalongkorn University; the thesis examiners: Associate Professor Dr. Nattaya Ngamrojanavanich, Department of Chemistry, Faculty of Science, Chulalongkorn University; Assistant Professor Dr. Vachiraporn Ajavakom, Department of Chemistry, Faculty of Science, Ramkhamhaeng University, for their invaluable discussion and suggestion.

I really appreciate Associate Professor Dr. Kiminori Matsubara, Department of Human Life Science Education, Graduate School of Education, Hiroshima University, Japan for anti-angiogenic activity. I would like to thank, Professor Dr. Kuniyoshi Shimizu, Department of Agro environmental Sciences, Faculty of Agriculture, Kyushu University and Shinrinken members for their help in providing facilities in the part cytotoxicity. Moreover, special thanks to the members of the laboratory (MHMK 1532), Department of Chemistry, Faculty of Science, Chulalongkorn University for their help and good friendship.

I wish to thank the Overseas Research Experience Scholarship for Graduate Student (G-RSAB) for supporting this research and the 90th Anniversary of Chulalongkorn University Fund (Ratchadaphiseksomphot Endowment Fund) for financial support to conduct this research.

CONTENTS

Page

Page

Page

LIST OF FIGURES

LIST OF SCHEMES

LIST OF TABLES

LIST OF ABBREVIATIONS

J	Coupling constant
δ	Chemical shift
δ_H	Chemical shift of proton
δ_C	Chemical shift of carbon
s	Singlet (for NMR spectra)
d	Doublet (for NMR spectra)
dd	Doublet of doublet (for NMR spectra)
t	Triplet (for NMR spectra)
m	Multiplet (for NMR spectra)
q	Quartet (for NMR spectra)
brs	Broad singlet (for NMR spectra)
qC	Quaternary carbon
calcd.	Calculated
^{1}H NMR	Proton nuclear magnetic resonance
^{13}C NMR	Carbon-13 nuclear magnetic resonance
2D NMR	Two dimensional nuclear magnetic resonance
^{1}H-^{1}H COSY	Homonuclear (proton-proton) correlation spectroscopy
NOESY	Nuclear overhauser effect spectroscopy
HSQC	Heteronuclear single quantum coherence

HMBC	Heteronuclear multiple bond correlation
ORTEP	Oak ridge thermal ellipsoid plot
HRESIMS	High resolution electrospray ionization mass spectrometry
CC	Column chromatography
TLC	Thin layer chromatography
IC_{50}	Half maximal inhibitory concentration
$CDCl_3$	Deuterated chloroform
MeOH	Methanol
EtOH	Ethanol
CH_2Cl_2	Dichloromethane
EtOAc	Ethyl acetate
DMSO	Dimethylsulfoxide
$(NH_4)_6Mo_7O_{24}$	Ammonium molybdate
H_2SO_4	Sulfuric acid
SiO_2	Silicon dioxide
g	Gram (s)
mg	Milligram (s)
mL	Milliliter (s)
μg	Microgram (s)
μL	Microliter (s)

μM	Micromolar
mM	Millimolar
L	Liter (s)
M	Molar
min	Minute
h	Hour
m	Meter (s)
mm	Millimeter (s)
cm	Centimeter (s)
nm	Nanometer
Hz	Hertz
MHz	Megahertz
cm^{-1}	Reciprocal centimeter (unit of wave number)
ppm	part per million
NMR	Nuclear magnetic resonance
MS	Mass spectrometry
IR	Infared
UV	Ultraviolet
$[M+Na]^{+}$	Pseudomolecular ion
λ_{max}	Wavelength of maximum absorption

c	Concentration
ε	Molar extinction coefficient
℃	Degree celcius
deg.	Degree
spp.	Species
No.	Number

CHAPTER I
INTRODUCTION

1.1 Angiogenesis in cancer

Nowadays, cancer is still enormous heath problem and cause dead rate tending to be increasing. Even though cancer can be found mostly in elder, it also can be found in any ages. Cancer is the disease occurred in cell scale, which normal cell evolves to disease cell infinitively and invades the normal neighbor cell. Thus, such disease can be happened in any part of body. In addition, cancer can be recognized to many different types. Presently, there are different kinds of cancer more than 100 types. Normally, therapies such as surgery, chemotherapy, radiation therapy, hormonal therapy that use to recover the health mostly have effects severely to our body. Thus, the new therapeutic approaches have to be developed in order to be more effective to fight against cancer [1].

Angiogenesis is the process of new capillary construction from the existing blood vessels in the body. Normally, such process is forced to happen when the body gets injury or pregnancy. However, this process is also crucial for the development and progression of cancer. When the tumor develops and grows until its diameter is more than 1-2 mm, nutrition and oxygen distribution cannot pass cell membrane to nourish cancer cell enough. Then, cancer starts to construct own angiogenesis to not only obtain oxygen and nutrition appropriately, and also have metabolism process in itself [2, 3]. Moreover, the new created vessel has a duty as tube to convey the cancer cell from its original position to distant sites in body. Consequently, cancer cell spreads and it is called “metastasis. Metastasis is the cause of more than 90% of human cancer deaths. Therefore, the new vessels growing the cancer can be suppressed; disease cell will not thrive and finally die.

More importantly, angiogenic process is the fundamental of every type of cancer growth, the drug that can inhibit such process must be used for all types of cancer or used as combination drug with chemotherapeutics [4, 5]. Recently, this method has attracted considerable attention from the researchers around the world.

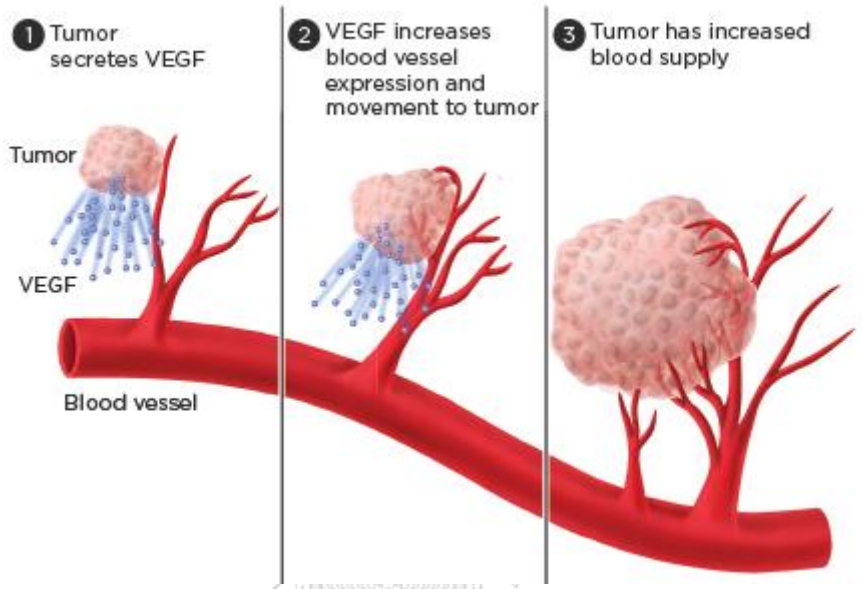

Figure 1.1 Blood vessel overgrowth on cell

(https://www.lungevity.org/about-lung-cancer/lung-cancer-101/treatment-options/angiogenesis-inhibitors)

Natural products are ongoing to be the key factor for research and development of novel chemical properties as drug-lead compounds. Separations of natural products are being increased by a lot of research groups around the world. All living organisms, fungi, bacteria, algae, animals and plants, generate various metabolites which compose of important primary metabolites for growth, evolution and breeding and secondary metabolites which are not significant for survival. Plants produce organic compounds that are not directly involved in growth, photosynthesis, reproduction or development. Secondary metabolites, on the other hand, play an important role in medicine, chemicals and so on [6, 7].

Among natural resources, plant-derived natural products are still being admitted to be the most important source for drug discovery and development [8]. A considerable proportion of plant-derived natural products used as drugs are from terrestrial plants offering an invaluable exhausted resource. Moreover, the ethanomedical knowledge from the use by human for several hundreds of years has been accumulated and proved for their less toxicity. In addition of being developed directly as drugs, these compounds also serve as lead structures/lead compounds to help to create the more effective drugs.

Mangrove, a kind of terrestrial plants growing along shore, has received much attention from natural product researchers due to the unique ecosystem [9]. In addition to growing in tropical areas, which provide great biodiversity, mangrove has to deal with changing tides and broad ranges of salinity, temperature, moisture and a number of other environmental factors. It is reasonable to expect that mangrove trees must be home to a great variety of bioactive secondary metabolites. This prompted us to embark on the study of bioactive metabolites from a Thai mangrove plant, *Derris trifoliata*.

1.2 Introduction of *Derris trifoliata*

Plants in the genus Derris belong to the order Fabales of the family Fabaceae. The plants are found throughout the tropical regions of Asian and East Africa. All parts of the plants, root, leaves, stem and bark, were found to have a kind of metabolite called rotenoids as major components.

Classification of *Derris trifoliata* [10]

Kingdom: Plantae

Division: Tracheophyta

Class: Magnoliopsida

Order: Fabales

Family: Fabaceae

Genus: Derris

Species: *Derris trifoliata*

Derris trifoliata is only one species of this genus which is classified as a mangrove plant and distributed throughout the mangrove forests of Thailand. It is an evergreen shrub, climbing stem and diameters to 4 cm. Blaze odour resembles that of freshly cut green beans. Leaves composed of 3-7 leaflets. Leaflets ovate to elliptic about 5.5-15 × 2.5-8 cm. Leaflet stalks about 0.6-1.2 cm long. Stipules are broadly triangular about 1-2 mm length. Its flowers are about 7-10 cm length and 1.3 cm diameter. Fruits flat about 3.5-5.5 × 2.2-2.8 cm, usually containing only 1 seed, rounded on the lower side and narrowly winged on the upper side its brown seeds are compressed, wrinkled and kidney-shaped. A plant of the moist, tropical lowlands, found in areas where the mean annual rainfall and the temperature can range from 20-29 $^{\circ}$C [11]. Various parts of *Derris trifoliata* are shown in **Figure 1.2.**

Figure 1.2 *Derris trifoliata*

(http://www.samunpri.com/ถอบแถบทะเล)

1.3 Literature reviews

Like other plants in the genus *Derris*, the previous chemical investigation of *D. trifoliata* has resulted in the isolation of rotenoids [12]. Rotenoids are isoflavonoid derivatives consisting of an extra carbon at the C-2 position connected to the C-2' though an ether linkage of form a tetracyclic ring system. They are occurring compounds of plant origin, particularly the genus *Millettia* and *Derris* (Leguminosae) [13] (**Figure 1.3**). Previous studies of rotenoids have shown their potential as anticancer, anti-inflammatory agents and as a pesticide, insecticide and acaricide [14, 15].

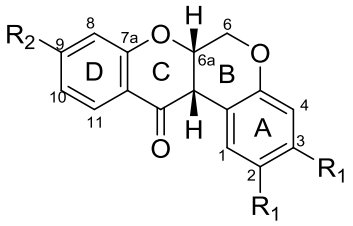

Figure 1.3 General structure of rotenoid

1.3.1 Rotenoids with anti-cancer activity

In 2004, Ito and co-workers reported the isolation and identification of six rotenoids (**1**-**6**) from the stems of *D. trifoliata* and five of them displayed cancer chemopreventive activity in the primary screening. Moreover, compounds **1** and **6** exhibited a marked inhibitory effect on mouse skin tumor promotion in an in vivo two-stage carcinogenesis test [16].

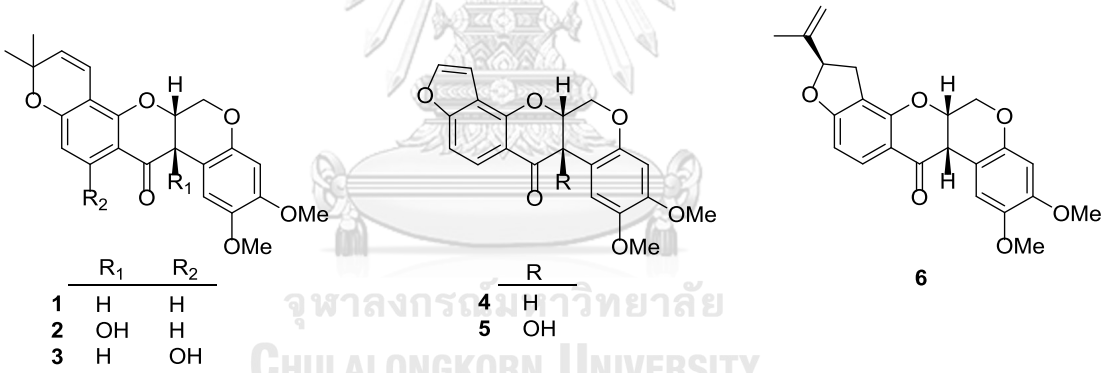

Figure 1.4 Rotenoids from stems of *D. trifoliata*

1.3.2 Rotenoids with larvicidal activity

Yesenew and co-workers (2006) reported the methanol crude extract of the seeds of D. *trifoliata* showed potent and dose dependent larvicidal activity against the 2nd instar larvae of *Aedes aegypti*. The isolation yielded six rotenoids (**5** and **7**-**10**), including two unusual rotenoids (**7** and **9**) [15].

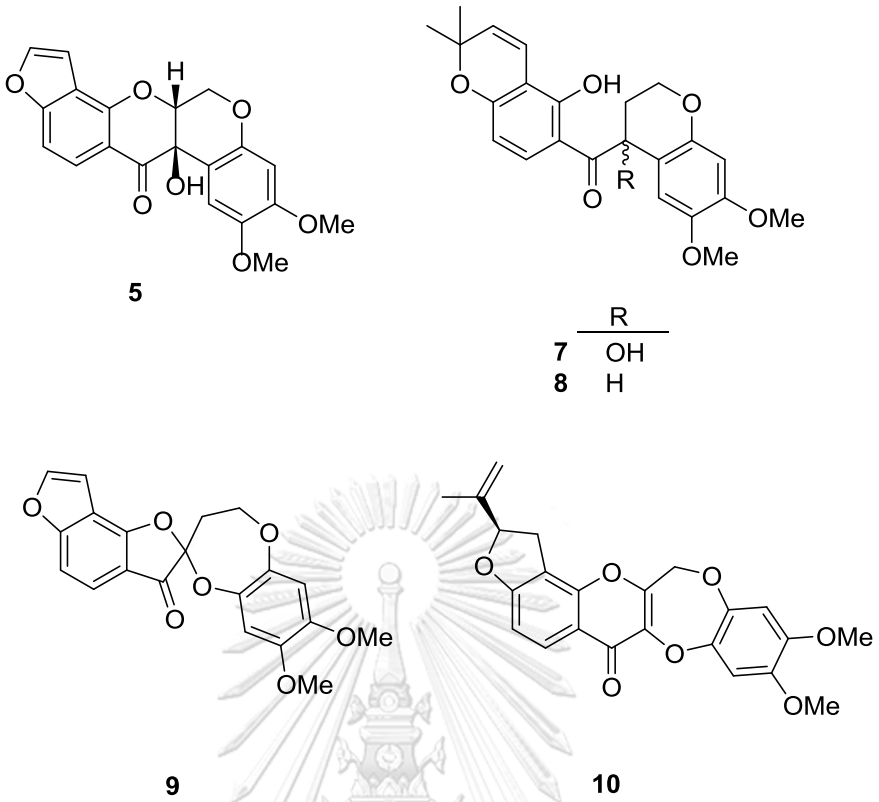

Figure 1.5 Rotenoids from seeds of *D. trifoliata*

1.3.3 Rotenoids with anti-inflammatory activity

Tewtrakul and co-workers (2009) described the isolation of nine rotenoids (**1-3, 5-6** and **11-14**) from the hexane and dichloromethane extracts of *D. trifoliata* stems and their nitric oxide (NO) inhibitory activity in RAW264.7 macrophage cells. All of them, except for compound **2**, showed promising anti-inflammatory activity with IC_{50} values ranging from 0.002-0.233 μM which was more active than positive controls, indomethacin (IC_{50} = 25.0 μM), caffeic acid phenethylester (IC_{50} = 5.6 μM) and L-nitroarginine (IC_{50} = 61.8 μM) [14].

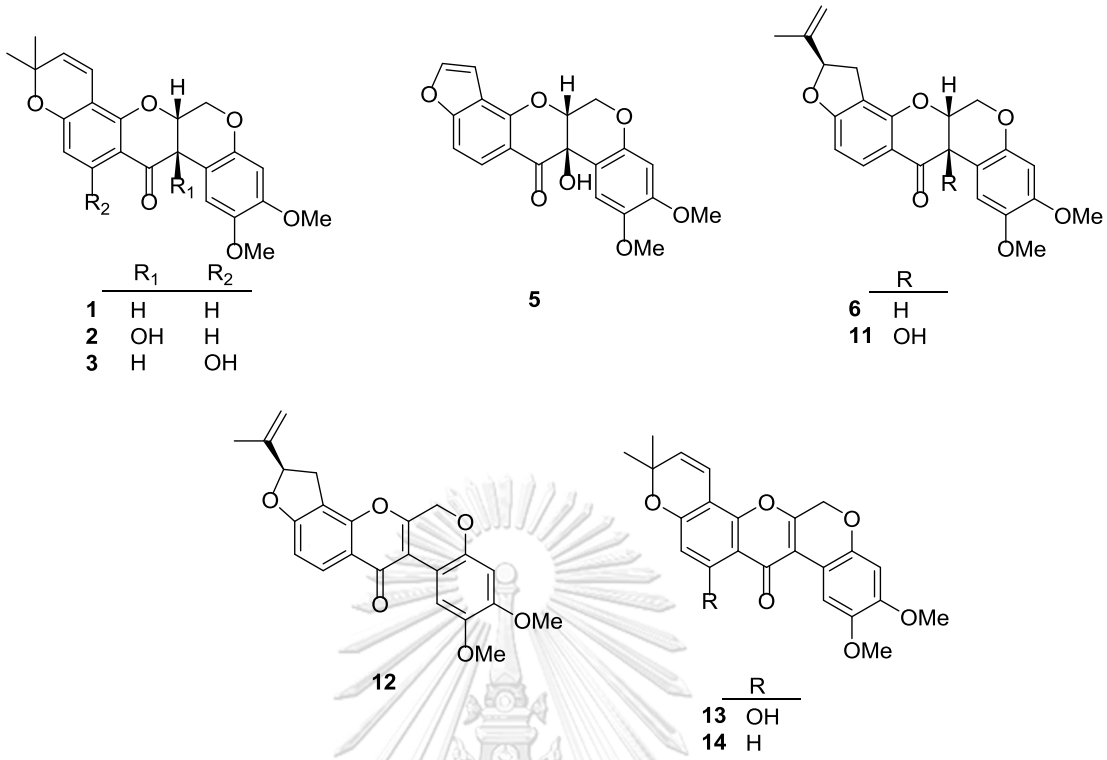

Figure 1.6 Rotenoids from the stems of *D. trifoliata*

1.3.4 Rotenoids with cancer chemopreventive activity

Ito and co-workers (2006) reported the isolation and identification of six rotenoids (**1**-**6**) from the acetone crude extract of stems of *D. trifoliata* and rotenoids **1**, **3**-**6** displayed cancer chemopreventive activity in the primary screening especially, rotenoid **5** displayed equivalent to that of ***β***-carotene without any cytotoxicity. Moreover, compound **1** and **3** exhibited a marked inhibitory effect on mouse skin tumor promotion in an in vivo two-stage carcinogenesis test [16].

1.3.5 Rotenoids with anti-angiogenic activity

In 2007, Kim and co-workers, studied anti-angiogenic effect of deguelin (**1**) on choroidal neovascularization. The results showed that deguelin could inhibit tube formation of human umbilical vein endothelial cells (HUVECs) in in vitro model and inhibit angiogenesis of chick chorioallantoic membrane (CAM) in in vivo model. In

addition, it was found that the compound did not show significant toxicity on cell viability of HUVECs in doses of 0.01 to 1 μM [17].

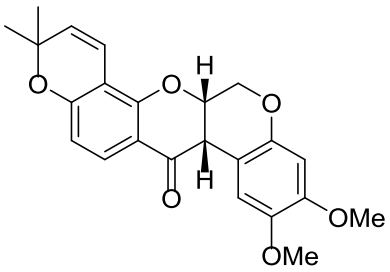

Figure 1.7 Structure of deguelin (**1**)

1.4 Objectives of the present study

Although some rotenoids from *D. trifoliata* have been reported to possess anti-cancer, cancer chemopreventive and anti-inflammatory activities, but their anti-angiogenic activity has been scarcely reported. Thus the present study focuses on isolation and identification of rotenoids from stems *D. trifoliata* to evaluate their anti-angiogenic activity. Therefore, the results of this study should provide new anti-angiogenic lead compounds.

Therefore, the objectives of this study are as follows;

1. To extract and isolate rotenoids from *D. trifoliata* stems
2. To elucidate structures of isolated rotenoids by spectroscopic techniques.
3. To evaluate their angiogenic inhibition and cytotoxic activities.
4. To study action mechanism of selected rotenoids on HUVECs function

CHAPTER II

EXPERIMENTS

2.1 Plant materials

Aerial part of *D. trifoliata* was collected from Chumphon, Thailand in October 2015. The plant was authenticated by the staff of Mu Ko Chumphon National Park.

2.2 General Experimental Procedures

2.2.1 Thin-layer chromatography (TLC)

Thin-layer chromatography (TLC) was performed on a sheet of aluminium foil which is coated with silica gel. Then TLC was observed with UV light at 256 nm wavelength and dipped with ammonium molybdate ($(NH_4)_6Mo_7)O_{24}$) in 5% H_2SO_4/EtOH.

2.2.2 Column chromatography

Column chromatography (CC) was performed using Silica gel 60H (Merck code No. 7734 and No. 9385) as packing materials.

2.2.3 Size exclusion chromatography

Size exclusion chromatography was performed by Sephadex LH-20 (Pharmacia Code No. 17-0090-01) to separate compounds according to their molecular weight.

2.2.4 High performance liquid chromatography (HPLC)

High performance liquid chromatography (HPLC) was performed using a Thermo Scientific Spectra System (Thermo Scientific P200 pump and Thermo Scientific UV6000LP detector). Column VertiSep^{TM} UPD C_{18} (4.6 × 150 mm, 5

μM) was used for analysis and Column GL Sciences (20 × 250 mm, 5 µM) was used for separation.

2.2.5 Nuclear magnetic resonance spectroscopy (NMR)

The NMR spectra were recorded in $CDCl_3$ using a Varian Mecury 400 plus (400 MHz for ^{1}H NMR) and a Bruker AV400 (400 MHz for ^{1}H NMR, 100 MHz for ^{13}C).

2.2.6 Mass spectrometry (MS)

HRESIMS spectra were obtained with a Bruker micrOTOF.

2.2.7 Ultraviolet-visible spectrophotometer (UV-vis)

UV data were recorded in MeOH on a POWERWAVE XS2 Biotek UV-Visble spectrophotometer.

2.2.8 Fourier transforms infrared spectrophotometer (FT-IR)

FT-IR spectra were recorded on a Perkin-Elmer Model 1760X Fourier Transform Infrared Spectrophotometer.

2.2.9 Microplate reader

MTT assay was measured at 570 nm using a BioTek™ ELx800™ Absorbance Microplate Readers.

2.3 Chemicals

2.3.1 Solvents

All commercial grade solvents, used in the present study, methanol (MeOH), acetone, ethyl acetate (EtOAc), dichloromethane (CH_2Cl_2) and n-hexane were purified by distillation prior to use. In addition, HPLC grade solvents, MeOH and Milli-Q water, were used for HPLC purification. The deuterated solvent for NMR experiments was $CDCl_3$.

2.4 Extraction and Isolation

Dried and powdered stems of *D. trifoliata* (5 kg) were extracted 3 times with MeOH (5 L, each for 3 days) at room temperature. The combined MeOH extract was concentrated under reduced pressure, and the residue was partitioned between water and EtOAc in equal amounts for 3 times. The EtOAc layer was combined and concentrated under reduced pressure to yield the EtOAc crude extract (112 g). The extraction procedure is shown in **Scheme 2.1**

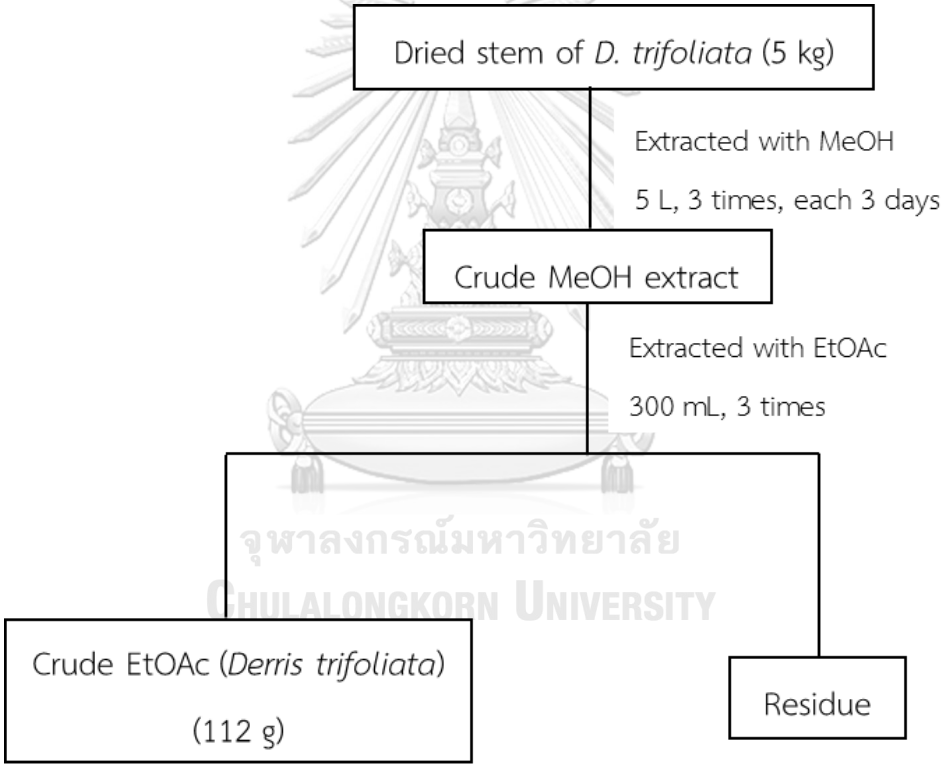

Scheme 2.1 Extraction of *D. trifoliata*

The EtOAc crude extract of *D. trifoliata* (112 g) was chromatographed over a SiO_2 column with gradient EtOAc: n-hexane (from 1:9 to 1:0), to give eight fractions, A-H. Fraction D (10.4632 g) was separated by SiO_2 column chromatography (CC) and

eluted with gradient of acetone: n-hexane mixture (from 1:4 to 7:3) yields seven subfractions (D1-D7). Subfractions D5 and D6 was recrystallized from MeOH to afford compound **12** (53.8 mg). The filtrate from D5 was subjected to Sephadex LH20 column chromatography (MeOH) to yield compound **6** (10.4 mg) and 11 subfractions (D5m1-D5m11). Fraction D5m9 was separated by preparative HPLC (GL Sciences, ODS-3, 20 × 250 mm, flow rate 8.00 mL/min, MeOH: H_2O, 2:3 to 9:1) to obtain compound **1** (8.4 mg).

Subfraction D7 (937.8 mg) was separated by SiO_2 CC using mixtures of MeOH: CH_2Cl_2 (from 1:49 to 1:19) to give 8 subfractions (D7a-D7h). Fraction D7c (347.2 mg) was rechromatographed with acetone: n-hexane (2:3) and the major fraction D7c.5 (45.0 mg) was purified by preparative HPLC (GL Sciences, ODS-3, 20 × 250 mm, flow rate 8.00 mL/min, MeOH: H_2O, 2: 3to 9:1) to obtain compounds **2** (4.7 mg) and **11** (10.1 mg). The isolation procedure is shown in **Scheme 2.2**

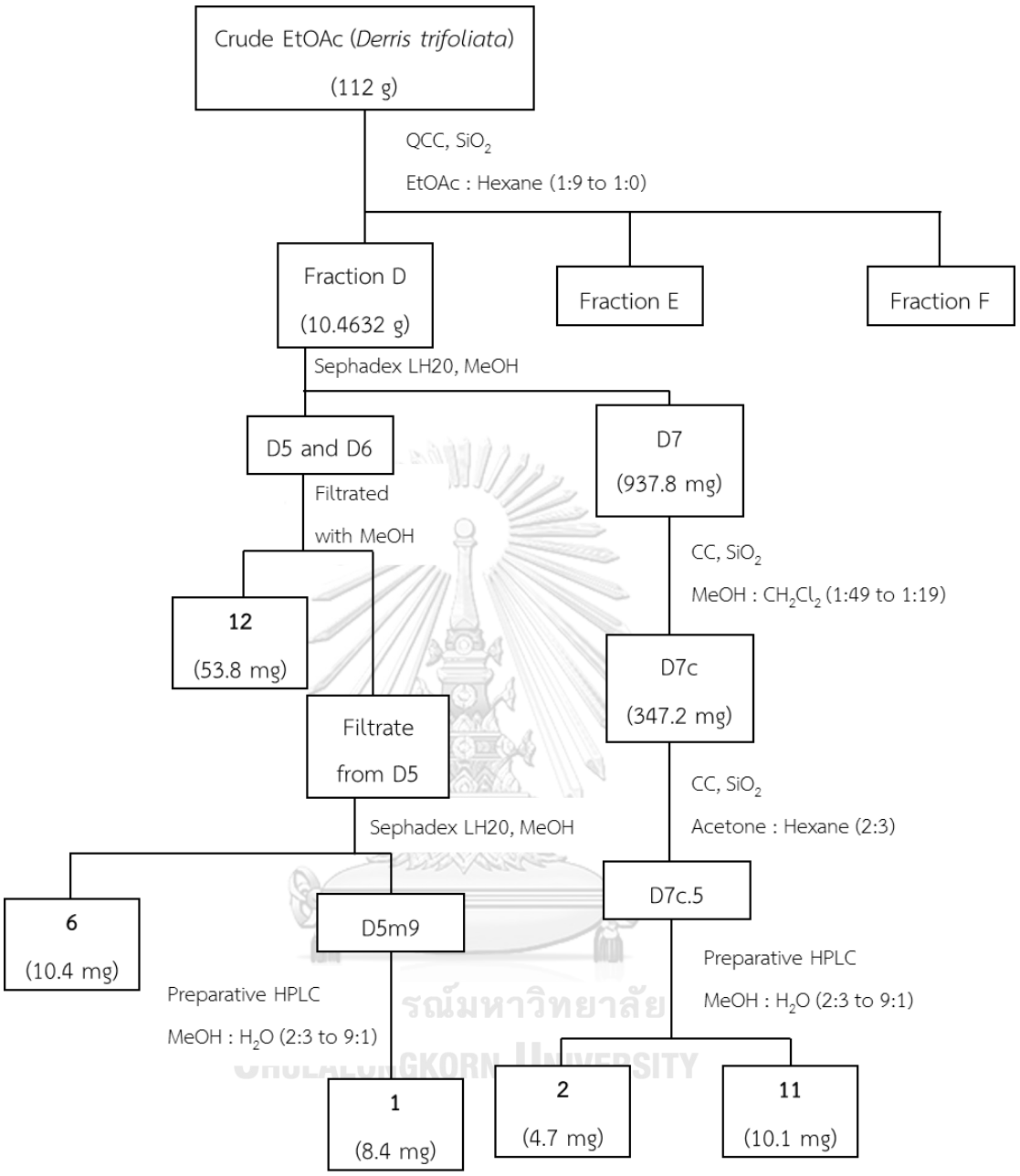

Scheme 2.2 Isolation procedure of Fraction D

Next, fraction E (5.4601 g) was chromatographed over a SiO_2 gel column with EtOAc: n-hexane (from 1:9 to 4:1) to afford 11 fractions (E1-E11). The 2.3859 g of fraction E11 was fractionated by sephadex LH20 column chromatography and eluted with MeOH to give six subfractions (E11a-E11f). Then fraction E11f (160.7 mg) was

purified by SiO_2 CC with EtOAc: CH_2Cl_2 mixtures (from 1:49 to 1:24) to afford compounds **4** (7.70 mg) and **5** (37.9 mg).

Fraction F (16.9998 g) was subjected to SiO_2 CC with gradients of acetone: n-hexane (from 1:9 to 1:0) to yield 11 subfractions (F1-F11). Then subfraction F9 (2.3209 g) was subjected to pass SiO_2 CC with EtOAc: CH_2Cl_2 (from 1:49 to 1:4) to give 12 fractions (F9a-F9l) and then fraction F9d (68.4 mg) was further purified by preparative HPCL (GL Sciences, ODS-3, 20 × 250 mm, flow rate 8.00 mL/min, MeOH: H_2O, 2:3 to 9:1) to afford compound **15** (6.6 mg). The isolation procedure is shown in **Scheme 2.3**

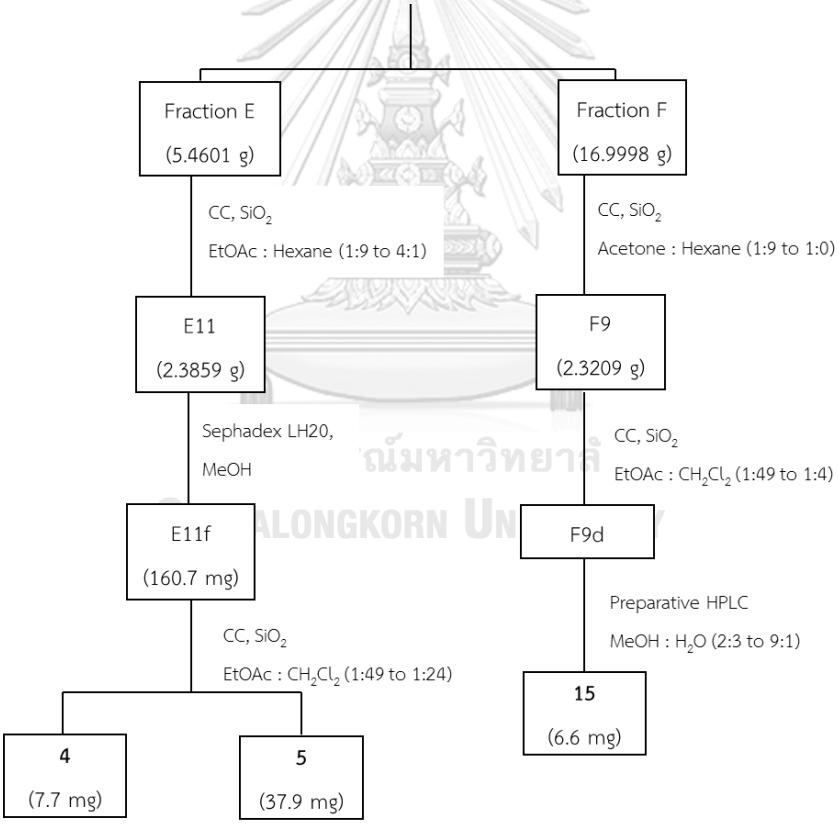

Scheme 2.3 Isolation procedure of Fractions E and F

2.5 Anti-angiogenic assay [18]

2.5.1 Ex vivo anti-angiogenic assay

A male Wistar rat was sacrificed by bleeding from the right femoral artery under anesthesia with diethyl ether. The thoracic aorta was removed, washed with RPMI 1640 medium, turned inside out and cut into length 1 mm. The aortic rings were replaced on 6-well culture plates and covered with 0.5 mL of gel maxtrix solution (8 volumes of porcine tendon collagen solution 1 volume of 10 × Eagle's MEM, and 1 volume of reconstitution buffer), then allowed to gel at 37 ^{o}C for 30 minutes. 2 mL of RPMI 1640 medium containing 1% of TIS+ with designated does of each compound or vehicle (DMSO) were added to the wells. After incubation for 7 days at 37 ^{o}C in 5% CO_2, capillary length was estimated by phase-contrast microscopy by measuring the distance from the cut end of the aortic segment to the approximate mid-point of the capillary. Further, compounds displaying potent activity were loaded to the assay at various concentrations and their IC_{50} values were determined.

2.5.2 In vitro anti-angiogenic assay

2.5.2.1 Tube formation assay

HUVEC tube formation assay was performed according to the method using BD Matrigel. Solid gel prepared on a 96-well tissue culture plate according to the manufacture's instruction. HUVECs (1 × 10^5 cells/mL) in HuMedia EG2 medium containing various doses of the compound or vehicle (DMSO) were seeded onto surface on solid BD Matrigel. After incubation for 12 h at 37 ^{o}C in 5% CO_2, tube formation was observed under an inverted light microscope at 40 × magnification. Microscopic fields were photographed with a digital camera.

2.5.2.2 Proliferation assay

A HUVEC suspension in HuMedia EG2 (1.5×10^4 cells/mL) was seeded onto each well of a 96-well plate (100 μL) and incubated for 24 h at 37 $^{\circ}$C in 5% CO_2. The medium was removed and replaced with fresh HuMedia EG2 containing various doses of the compound or vehicle (DMSO) and incubated for 72 h at 37 $^{\circ}$C in 5% CO_2. Cell proliferation was detected using WST-8 reagent and the incubation of proliferation was measured at 450 nm using a microplate reader.

2.5.2.3 Chemotactic migration assay

HUVEC migration assay was performed using a modified Boyden chamber. A microporous membrane (8 μm) of 24-well cell culture inserts was coated with 0.1% gelatin. A HUVEC suspension in Medium 199 with 0.1% bovine serum albumin (BSA) (2.5×10^5 cells/mL) was seeded in each chamber (400 μL). The well was filled with 400 μL of Medium 199 containing 0.1% BSA and 10 ng/mL of human recombinant VEGF with or without the compound. The assembled chamber was incubated for 6 h at 37 $^{\circ}$C in 5% CO_2. Non-migrated cells on the surface of the membrane were removed by scrubbling with the cotton swab. The migrated cells were fixed with methanol and stained with Diff-Quik stain, then counted in three fields of each membrane under microscope at 200 × magnification.

2.6 Cell culture

All cell lines, except for HUVEC, were obtained from Riken Bio resource Center of Japan (Ibaraki, Japan). Human cervical carcinoma (CaSki) cells were cultured in RPMI-1640 medium, and colon cancer (HCT-116), hepato carcinoma (Hep-G2) and normal human colon epithelial (CCD841) cells were cultured in Dulbecco's

Modified Eagle's medium (DMEM) at 37 ^{o}C in a 5% CO_2 humidified incubator. Both media were supplemented with 10% FBS, 2 mM L-glutamine, 100 U/mL of penicillin and 100 mg/mL of streptomycin. HUVECs were obtained from Kurabo Industries (Osaka, Japan) and the cells were cultured in HuMedia EG2 medium supplemented with 2% FBS, 10 ng/mL of recombinant human epidermal growth factor (bFGF), 1 μg/mL of hydrocortisone and 10 μg/mL of heparin at 37 ^{o}C in a 5% CO_2 humidified incubator.

2.7 Cytotoxic activity [19], [20]

Bioassay of cytotoxic activity was performed *in vitro* by calorimetric method that measures the reduction of MTT (3-(4,5-dimethylthiazol-2-yl)-2,5-diphynyltrazolium bromide) by mitochondrial succinate dehydrogenase. The MTT enters cells and passes into the mitochondria, it is reduced to dark purple (formazan), followed by solubilization and measurement by spectrophotometry. Generally, reduction of MTT occurs in metabolically active cells, the level of activity is thus measured from the viability of the cell, which is proportional.

The cells were cultured from tissue culture dishes, counted and seed cells in a 96-wells plate at a densities of 1x10^{4} cells/well in 100 μL. Cells were incubated in a 5% CO_2 at 37 ^{o}C, for 24 h. After removed the medium and washed cells with PBS, the cells were treated with six different concentrations of the isolated compounds, dissolved in DMSO. Doxorubicin (TCI, > 98% by HPLC) was used as positive control. After 72 h, cell viability was determined using MTT reagent as follows: 10 μL of MTT solution (5 mg/mL PBS) was added to each well, followed by 4 h incubation at 37 ^{o}C in 5% CO_2, then supernatant was discarded and DMSO (100 μM) was added to dissolve formazan crystals. The absorbance was measured at 570 nm using a Microplate Reader.

The results were presented as the percentage of inhibition and the half maximal inhibitory concentration (IC_{50})

Calculation of the percentage of cell viability

$$\% \text{ cell viability} = \frac{\text{Absorbance of tested cells}}{\text{Absorbance of control cells}} \times 100$$

2.8 Wound-healing assay

HCT-116 cell migration was determined using wound-healing assay. Cells were seeded into a 24-wells plate with a density of 2.5 x 10^5 cells/well. After the cell monolayer was formed, a 1 mm micropipette tip was used to scratch the attached cells to generate a wound space. Then, the cells were washed with PBS and replaced with serum-free medium containing various concentrations of 11. The cells were photographed at 0 and 24 h using an inverted microscope. The progress of the cell migration into the wound was then calculated.

2.9 Statistical analysis

Data are expressed as mean values and standard deviation. Significance was analyzed by one-way analysis of variance and Dunnett's multiple comparison tests by GraphPad Prism 5.01. A p-value of < 0.05 was considered statistically significance.

CHAPTER III

RESULTS AND DISCUSION

3.1 Isolated rotenoids from *D. trifoliata* stem

The EtOAc crude extract of *D. trifoliata* stem was purified by chromatographic techniques to afford eight rotenoids, namely deguelin (**1**), tephrosin (**2**), elliptone (**4**), 12a-hydroxyelliptone (**5**), rotenone (**6**), 12a-hydroxyrotenone (**11**), 6a, 12a-dehydrorotenone (**12**), and 7a-*O*-methylelliptonal (**15**). Their structures (**Figure 3.1**) were established by 1D and 2D NMR analysis and by comparing the NMR data with those reported in the literature.

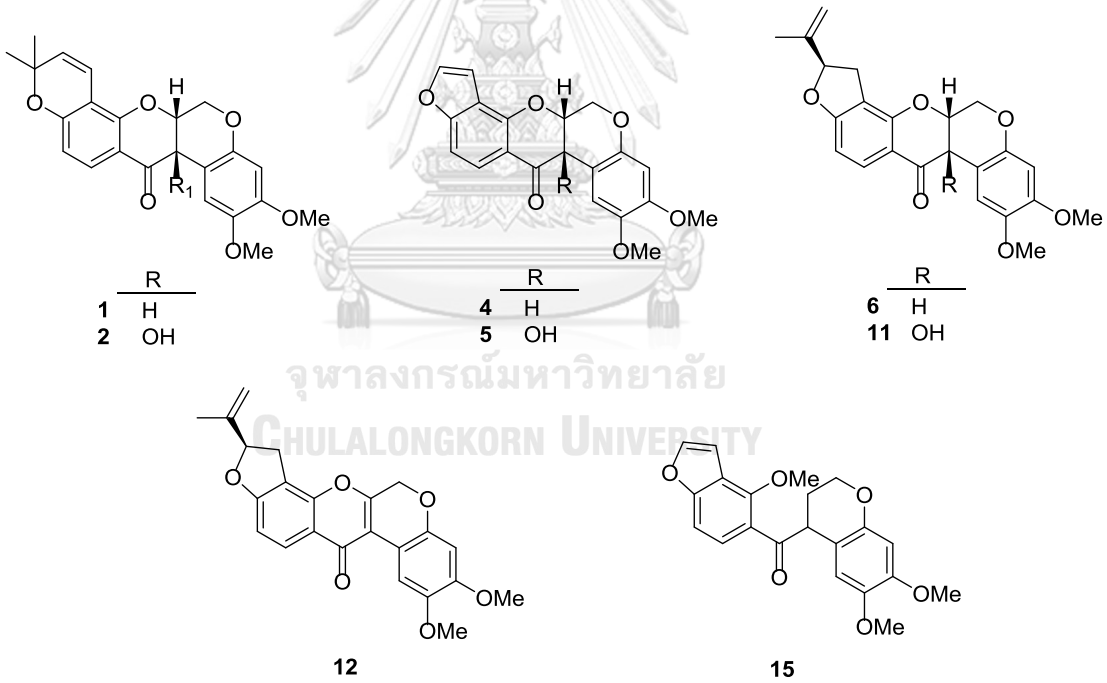

Figure 3.1 Structures of isolated rotenoids from *D. trifoliata* stem

3.2 Structure elucidation of isolated rotenoids

3.2.1 Structure elucidation of compound **1**

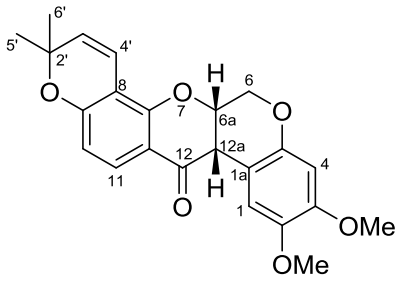

Figure 3.2 Structure of compound **1**

Compound **1** was obtained as orange-yellow solid, UV (MeOH) λ_{max} (log ε) 270 (5.44) nm, IR (neat): 1608 cm^{-1}, and its molecular formula $C_{23}H_{22}O_6$ was deduced from its NMR data. Analysis of ^{1}H-NMR (**Table 3.1**), ^{13}C-NMR (**Table 3.2**) and HSQC data revealed that the molecule of **1** contained one carbonyl carbon (δ_C 189.2), two methoxyls (δ_H 3.77 s, 3.80 s; δ_C 56.3 and 55.8), one oxygenated methylene (δ_H 4.20 d, *J* = 12.0 Hz, 4.65 dd, J = 12.4, 3.2 Hz; δ_C 66.3), two tertiary methyls (δ_H 1.35 s, 1.44 s; δ_C 28.6, 28.8), one oxygenated methine (δ_H 4.92 d, *J* = 6.0 Hz; δ_C 72.4), one methine (δ_H 3.84 d, *J* = 3.6 Hz; δ_C 44.4), one oxygenated quaternary carbon (δ_C 76.8), a carbon-carbon double bond (δ_H 5.55, 6.66 each d, *J* = 10.0 Hz), and two aromatic rings. Two methoxy groups were positioned at C-2 and C-3 due to HMBC correlations of their protons to C-2 and C-3, and two tertiary methyls were attached to the same carbon C-2**'** based on their HMBC correlations as shown in **Figure 3.3**. The structure was further confirmed by the ^{1}H-^{1}H COSY and HMBC correlations including correlations of H-6/H-6a, H-6a/H-12a, H-10/H-11, H-3**'**/H-4**'**, H-6/C-12a, H-6a/C-1a, H3**'**/C-8, H4**'**/C-9 (**Figure 3.3**). Moreover, the structure of **1** was confirmed by comparison of its NMR data to those previously reported, and it was identified as deguelin [21].

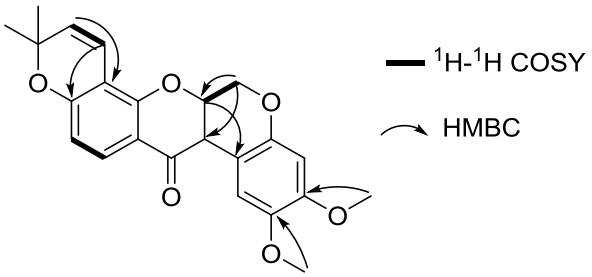

Figure 3.3 HMBC and ^{1}H-^{1}H COSY correlations of compound **1**

3.2.2 Structure elucidation of compound **2**

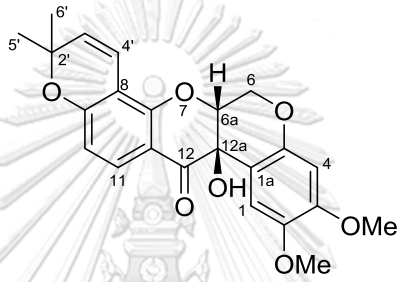

Figure 3.4 Structure of compound **2**

Compound **2** was obtained as yellow amorphous powder, UV (MeOH) λ_{max} (log ε) 260 (5.49) nm, IR (neat): 3458, 1615 cm^{-1} and the molecular formula $C_{23}H_{22}O_7$ was established by 1D and 2D NMR. The NMR spectra of compound **2** (**Tables 3.1** and **3.2**) were very similar to those of compound **1**, except for the existence of an additional oxygenated quaternary carbon (δ_C 76.4) and a hydroxyl group (δ_H 4.57), replacing the CH-12a in compound **1**. This was further confirmed by HMBC correlations of 12a-OH to C-12a, C-12, and C-1a (**Figure 3.5**). By comparison of its NMR data with those reported in the literature [16], compound **2** was identified as tephrosin.

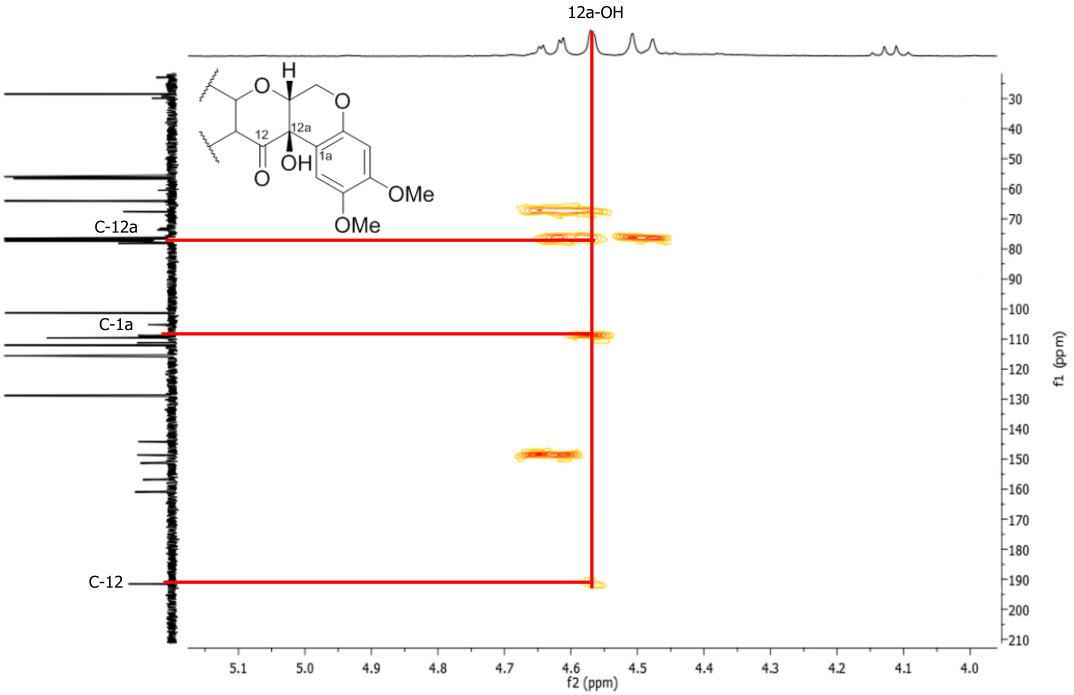

Figure 3.5 Key HMBC correlation of compound **2** in $CDCl_3$

3.2.3 Structure elucidation of compound **4**

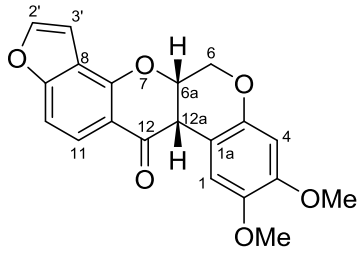

Figure 3.6 Structure of compound **4**

Compound **4** was obtained yellowish paste, UV (MeOH) λ_{max} (log ε) 260 (5.43) nm, IR (neat): 2929, 2352, 1609 cm^{-1} and had the molecular formula $C_{20}H_{16}O_6$, determined by analysis of ^{1}H-NMR and ^{13}C-NMR data. The NMR data of **4** (**Tables 3.1** and **3.2**) also exhibited typical signals for rotenoid skeleton, and were similar to those of compound **1**, except for the absence of signals for gem-dimethyl functionality (qC-2**'**, Me-5**'** and Me-6**'**) appeared in compound **1**. The chemical shift of a CH-2**'** double bond at δ_C 142.5 implied that this carbon connected with an oxygen containing moiety. Based on this data and the number of protons and carbons, the ring E of **4** should be a furan ring. The structure was confirmed by comparing its NMR data with those previously reported, and compound **4** was a known rotenoid, elliptone, previously reported by Ngandeu et al. [22].

3.2.4 Structure elucidation of compound **5**

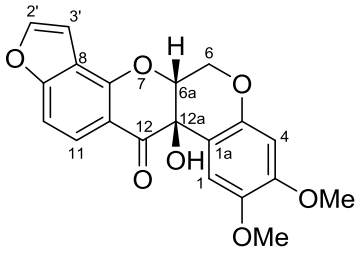

Figure 3.7 Structure of compound **5**

Compound **5** was isolated as a yellowish paste, UV (MeOH) λ_{max} (log ε) 260 (5.44) nm and IR (neat): 3449, 1606 cm^{-1}. Its molecular formula was assigned as $C_{20}H_{16}O_7$ based on its ^{1}H and ^{13}C NMR data. NMR spectra of compound **5** were very similar to those of compound **4.** The major difference between these two compounds was the absence of a methine proton H-12a in compound **4**, and the appearance of the signal for a hydroxyl group at δ_H 4.75 in compound 5 as shown in **Figure 3.8**. It suggested that the CH-12a of **4** was replaced by the qC-OH in **5**. Thus compound **5** was identified as 12a-hydroxyelliptone, which was further confirmed by comparing its NMR data to those in the literature [11].

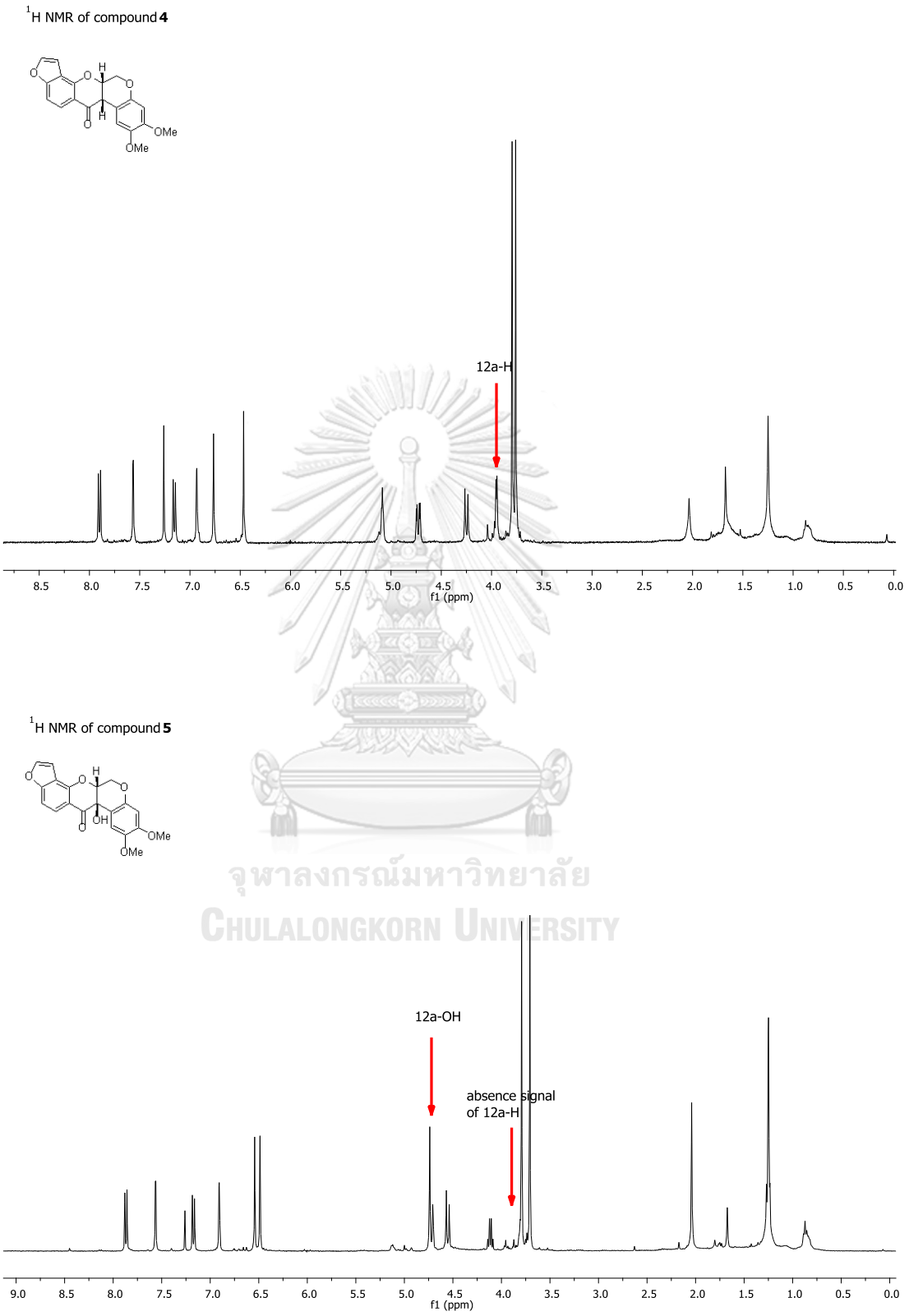

Figure 3.8 Comparison of ^{1}H NMR spectra of compounds **4** and **5** in $CDCl_3$

Table 3.1 ^{1}H NMR data of compounds **1**, **2**, **4** and **5** in $CDCl_3$

Position	δ_H (ppm), mult, (*J* in Hz)			
	1	**2**	**4**	**5**
1	6.79, s	6.48, s	6.76, s	6.54, s
1a				
2				
3				
4	6.45, s	6.55, s	6.46 s	6.48, s
4a				
6	4.65, dd, 12.4, 3.2 4.20, d, 12.0	4.64, dd, 12.0, 2.4 4.48, d, 12.0	4.74, dd, 12.0, 2.8 4.26, d, 12.0	4.70, dd, 11.6, 2.4 4.56, dd, 11.6
6a	4.92, t, 6.0		5.09, t, 6.8	4.73, brs
7a				
8				
9				
10	6.46, d, 8.8	6.45, d, 8.8	7.16, d, 8.8	7.18, d, 8.8
11	7.75, d, 8.8	7.72, d, 8.8	7.91, d, 8.8	7.87, d, 8.4
11a				
12				
12a	3.84, d, 3.6		3.95, d, 3.6	
2-OMe	3.77, s	3.81, s	3.79, s	3.70, s
3-OMe	3.80, s	3.73, s	3.76, s	3.79, s
2'			7.56, d, 2.0	7.56, d, 2.0
3'	5.55, d, 10.0	5.55, d, 10.4	6.93, d, 1.6	6.90, d, 1.2
4'	6.66, d, 10.0	6.59, d, 10.0	-	-
5'	1.35, s	1.38, s	-	-
6'	1.44, s	1.44, s	-	-
12a-OH	-	4.57, brs	-	4.73, brs

Table 3.2 ^{13}C NMR data of compounds **1**, **2**, **4** and **5** in $CDCl_3$

Position	δ_C (ppm)			
	1	**2**	**4**	**5**
1	110.5	101.2	109.0	109.5
1a	104.8	108.4	102.8	108.6
2	149.3	151.3	141.7	144.2
3	149.5	144.1	147.4	151.4
4	100.9	109.6	100.0	101.3
4a	147.4	148.5	145.0	148.6
6	66.3	64.0	65.0	63.9
6a	72.4	67.6	72.0	76.9
7a	156.9	156.8	157.5	155.8
8	109.1	109.2	111.2	117.4
9	160.1	160.9	159.2	160.8
10	111.4	112.0	104.8	107.2
11	126.6	128.7	122.0	124.0
11a	112.7	111.2	115.5	112.2
12	189.2	191.5	186.5	192.3
12a	44.4	76.4	44.0	67.9
2-OMe	56.3	56.0	54.9	56.5
3-OMe	55.8	56.5	55.0	56.0
2'	76.8	78.1	142.5	145.2
3'	128.0	128.9	103.0	104.9
4'	115.7	115.5	-	-
5'	28.6	28.4	-	-
6'	28.8	28.6	-	-

3.2.5 Structure elucidation of compound **11**

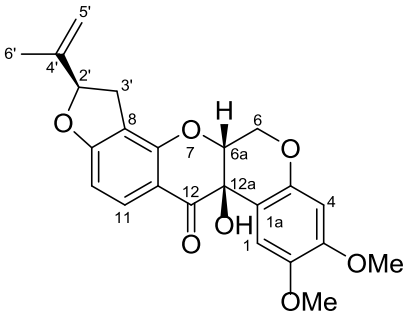

Figure 3.9 Structure of compound **11**

Compound **11** was obtained as a yellow amorphous powder, UV (MeOH) λ_{max} (log ε) 260 (5.49) nm, IR (neat): 3448, 1596 cm^{-1} and had a molecular formula $C_{23}O_{22}O_7$ established by 1D and 2D NMR. By considering its ^{1}H-NMR and ^{13}C-NMR spectra (**Table 3.3**), it was found that compound **11** shared the structure of rings A to D with compounds **2** and **5**, these compounds differed each other only at the structure of E ring. For compound **11**, its NMR data revealed that the E ring comprised of one tertiary methyl (δ_H 1.82 s; δ_C 17.2), one oxygenated methine (δ_H 5.23 t, *J* = 8.8 Hz; δ_C 17.2), one methylene (δ_H 2.93 dd, J = 15.6, 8.4 Hz, 3.28 dd, J = 15.6, 10.0 Hz; δ_C 31.2) and a terminal double bond (δ_H 4.93 s, 5.06 s; δ_C 112.8 CH_2, 143.0 qC). ^{1}H-^{1}H COSY correlation of H-2**'**/H-3**'** and the chemical shift of C-2**'** at δ_C 88.1 led to the formation of the five-membered E ring. An isopropenyl moiety was positioned at C-2**'** owing to HMBC correlations of H_2-5**'**/C-6**',** H_2-5**'**/C-4**',** H_2-6**'**/C-4**',** H_2-5**'**/C-2**'** and H_2-6**'**/C-2**'** (**Figure 3.10**). The structure of compound **11** was established as shown in **Figure 3.9** and it was identified as 12a-hydroxyrotenone [23]. The chemical structure was confirmed by comparing its NMR data to those in the literature.

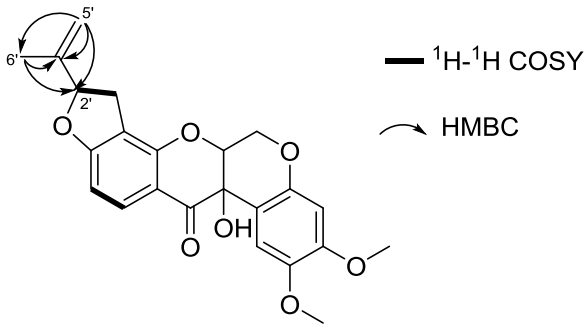

Figure 3.10 HMBC and ^{1}H-^{1}H COSY correlations of compound **11**

3.2.6 Structure elucidation of compound **6**

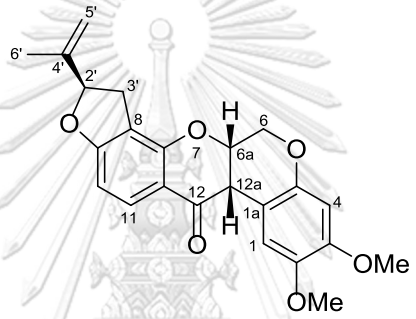

Figure 3.11 Structure of compound **6**

Compound **6**, was isolated as a white powder, UV (MeOH) λ_{max} (log ε) 260 (5.48) nm, IR (neat): 1601 cm^{-1} and its molecular formula as $C_{23}O_{22}O_6$ was determined by ^{1}H-NMR and ^{13}C-NMR data (**Tables 3.3** and **3.4**). NMR spectra of compound **6** was almost identical to those of compound **11**, except for the appearance of an additional methine in **6** in place of the C-12a oxygenated methine in **11**. Hence, compound **11** was identified as rotenone which was further confirmed by comparison of its NMR data to those previously reported.

3.2.7 Structure elucidation of compound **12**

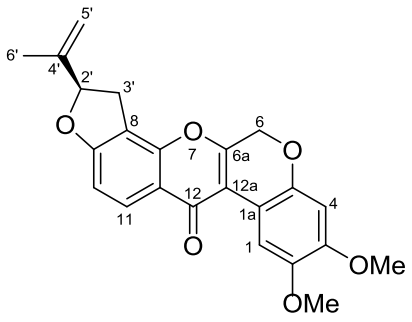

Figure 3.12 Structure of compound **12**

Compound **12** was obtained as yellow crystals, UV (MeOH) λ_{max} (log ε) 230 (5.47) nm, IR (neat): 2916, 2352, 1604 cm^{-1}, and the molecular formula $C_{23}H_{20}O_6$ was determined according to 1D and 2D NMR data (**Tables 3.3** and **3.4**). NMR spectra of compound **12** were very similar to those of compounds **6** and **11**, with the only difference in being the existence of an additional C-6a and C-12a double bond in **12** replacing a C-6a and C-12a single bond in **6** and **11**. The upfield shift of the carbonyl carbon to δ_C 174.5 supported the presence of the double bond at this position shown in **Figure 3.13**. Moreover, the complete structure of compound **12** was confirmed by ^{1}H-^{1}H COSY and HMBC correlations and it was identified as 6a, 12a-dehydrorotenone [24].

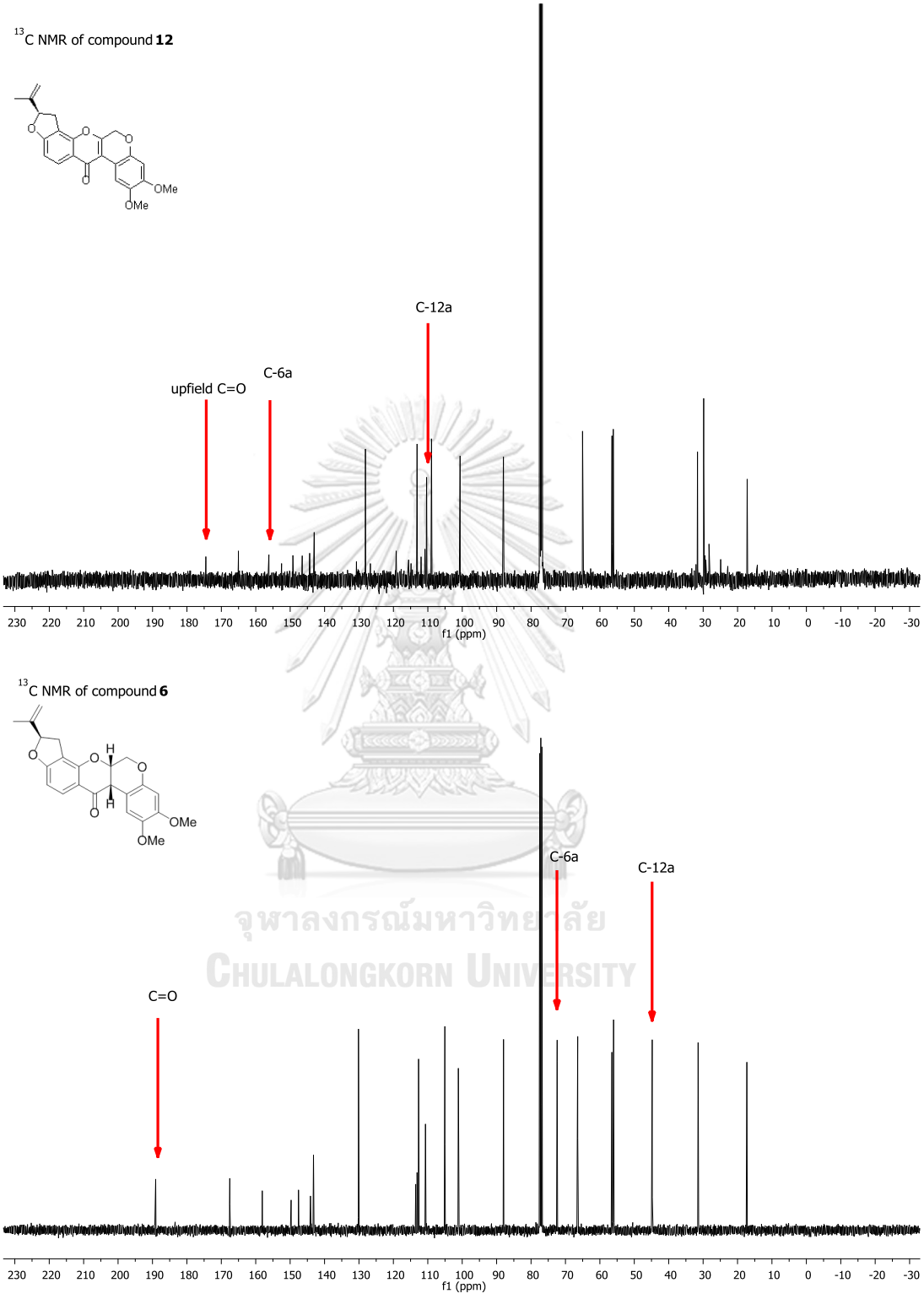

Figure 3.13 Comparison of ^{13}C NMR spectra of compounds **6** and **12** in $CDCl_3$

3.2.8 Structure elucidation of compound **15**

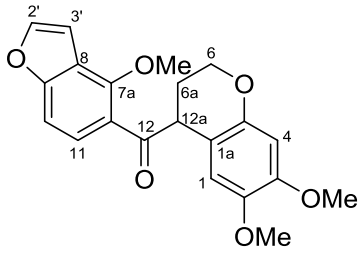

Figure **3.14** Structure of compound **15**

Compound **15** was obtained brown paste, UV (MeOH) λ_{max} (log ε) 260 (5.44) nm, IR (neat): 2929, 1595 cm^{-1}, and had a molecular formula $C_{21}H_{20}O_6$ established by HRESIMS ion at *m/z* 391.12969 $[M - Na]^+$ (calcd 391.11521). The NMR spectroscopic data of compound **15** (**Tables 3.3** and **3.4**) were close to those of compound **4**; however, the pattern of NMR data of rings B and C was different. Its NMR displayed an additional methoxy group (δ_H 4.18 s, δ_C 60.7), which was attached to C-7a due to HMBC correlation of 7a-OMe/C-7a. This indicated that the C ring of **15** must be broken by breaking the bond between C-6a and O atom. In addition, the NMR data of **15** revealed the presence of an additional methylene (δ_H 2.24 m; δ_C 25.4), which was assigned to C-6a, in place of a C-6a oxygenated methane in **6** and **11**. This was confirmed by ^1H-^1H COSY correlations of H_2-6a with H-6 and H-12a as shown in **Figure 3.15**. From these results, the structure of **15** was identified as 7a-*O*-methylelliptonal of which its NMR data matched with those in the literature [25].

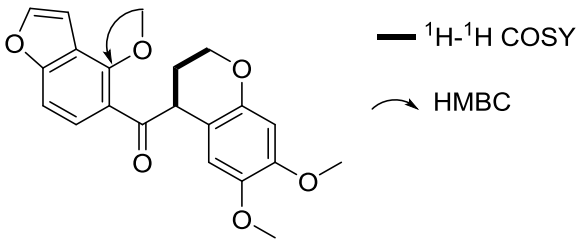

Figure 3.15 HMBC and ^1H-^1H COSY correlations of compound **15**

Table 3.3 ^{1}H NMR data of compounds **6**, **11**, **12** and **15** in $CDCl_3$

Position	δ_H (ppm), mult. (*J* in Hz)			
	6	**11**	**12**	**15**
1	6.76, s	6.54, s	8.45, s	6.39, s
1a				
2				
3				
4	6.44 s	6.48, s	6.55, s	6.42, s
4a				
6	4.62, dd, 12.0, 2.8	4.61, d, 2.4	5.00, t, 10.0	4.19, m
	4.18, d, 12.0	4.48		
6a	4.92, brs	4.58, s		2.24, m
7a				
8				
9				
10	6.59, d, 8.4	6.52, d, 8.8	6.92, d, 8.4	7.24, d, 8.8
11	7.83, d, 8.4	7.82, d, 8.4	8.13, d, 8.4	7.46, d, 8.8
11a				
12				
12a	3.83, d, 3.6			4.68, t, 5.6
2-OMe	3.80, s	3.81, s	3.95, s	3.60, s
3-OMe	3.76, s	3.72, s	3.87, s	3.81, s
2'	5.22, t, 9.2	2.93, dd, 15.6, 8.4	5.41, t, 8.8	7.64, d, 1.6
		3.28, dd, 15.6, 10.0		
3'	3.31, dd, 16.0, 10.0	5.23, t, 8.8	3.53, dd, 15.6, 9.6	7.02, d, 1.6
	2.95, dd, 16.0, 8.4		3.19, dd, 15.6, 8.0	
4'				-
5'	5.06, s	4.93, s	5.14, s	-
	4.92, s	5.06, s	4.98, s	
6'	1.76, s	1.80, s	1.80, s	-
7a-OMe	-	-	-	4.18 s

Table 3.4 ^{13}C NMR data of compounds **6**, **11**, **12** and **15** in $CDCl_3$

Position	δ_C (ppm)			
	6	**11**	**12**	**15**
1	110.6	109.6	110.3	113.1
1a	105.0	108.9	110.8	110.7
2	144.1	144.1	144.3	143.1
3	149.7	151.3	149.0	149.4
4	101.1	101.2	100.6	101.1
4a	147.5	148.5	146.4	149.3
6	66.4	64.0	65.0	63.7
6a	72.4	76.2	156.0	25.4
7a	158.0	157.8	152.5	152.8
8	113.1	113.3	113.1	125.2
9	167.5	168.1	165.0	159.0
10	105.0	105.4	108.0	106.7
11	130.1	130.2	128.1	126.6
11a	113.5	111.9	119.1	118.1
12	189.0	174.5	174.5	204.5
12a	44.7	67.7	111.9	45.9
2-OMe	56.5	56.0	56.4	56.4
3-OMe	56.0	56.5	56.1	55.9
2'	88.0	88.1	88.0	145.0
3'	31.4	31.2	31.6	105.6
4'	143.2	143.0	143.0	-
5'	112.6	112.8	113.1	-
6'	17.2	17.2	17.2	-
7-OMe	-	-	-	60.7

3.3 Cytotoxic activity

Cytotoxic effects of rotenoids against cancer cells seem to be most pronounced; however, their effects on cancer cell migration and angiogenesis, which play a crucial role during metastasis, are seldom investigated. To determine the effect of the compounds on cancer cells, their cytotoxicity against three human cancer cell lines, cervical carcinoma (CaSki), colon cancer (HCT-116), and hepato carcinoma (Hep-G2) cells, was investigated, and cell viability was examined by the MTT assay. Doxorubicin was used as a positive control. As shown in **Table 3.5**, compounds **1**-**2, 6** and **11** displayed promising activity against HCT-116 with IC_{50} values of 0.36, 0.51, 0.12 and 0.25 μM, respectively, while they showed weak toxicity on Hep-G2. In addition, compounds **4**-**5** and **15** were less active or inactive against all three cancer cell lines, as well as all isolated compounds did not show any significant activity on CaSki. Previous study has been reported that rotenoids not only containing a planar moiety, but also having a bent shape conformation between C-6a to C-12a play an important role in their anti-proliferation against cancer cells [26].

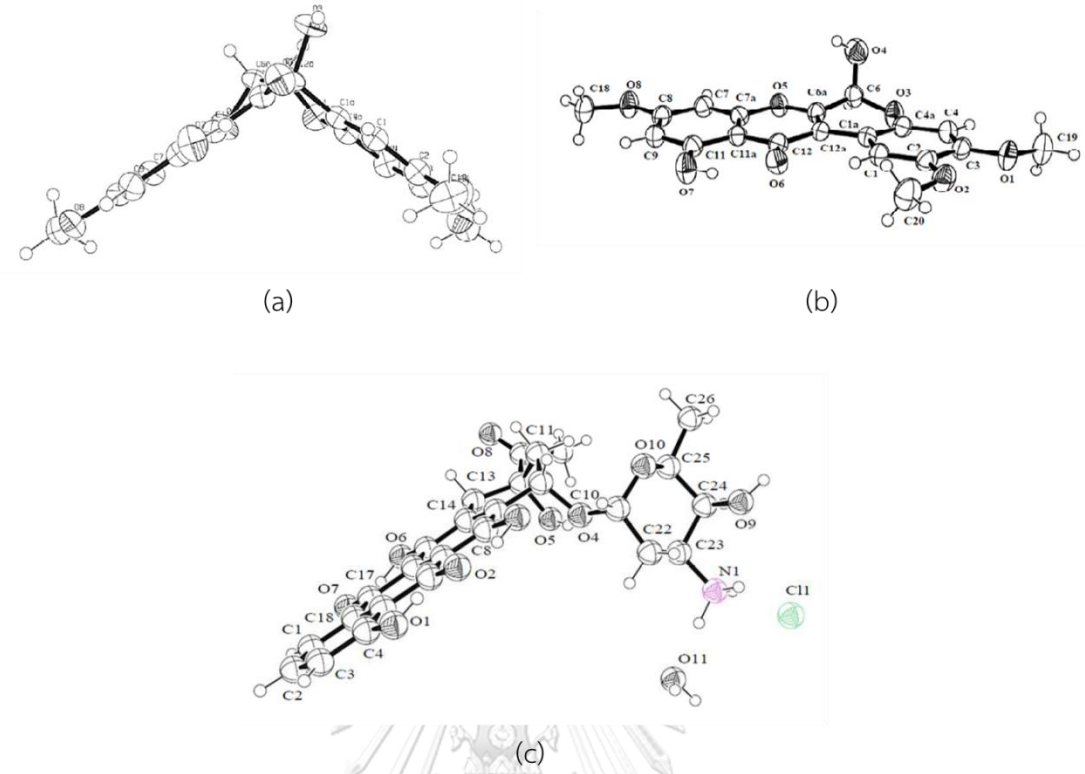

Figure 3.16 ORTEP structure showed top view of 6-deoxyclitoriacetal (a) stemonal (b) and doxorubicin HCl (c)

The doxorubicin, standard drug, rotenoids **6** and **11** have ability in the same, having a planar polycyclic part be able to intercalate into the space between two adjacent base pairs of DNA and inhibited the transcription and replication process. The position C6a-C12a is the only difference between molecular structure of rotenoid **12** and rotenoids **6** and **11**. In rotenoid **12** structure, there is a double bond at C6a-C12a position making it planar, while having the single bond at the same position in rotenoid **6** and **11** structures cause its bent shape [26]. This evidence helped to explain that compounds **1**-**2**, **6** and **11** were considerably potent over compound **12** possessing only a planar structure (**Figure 3.17**).

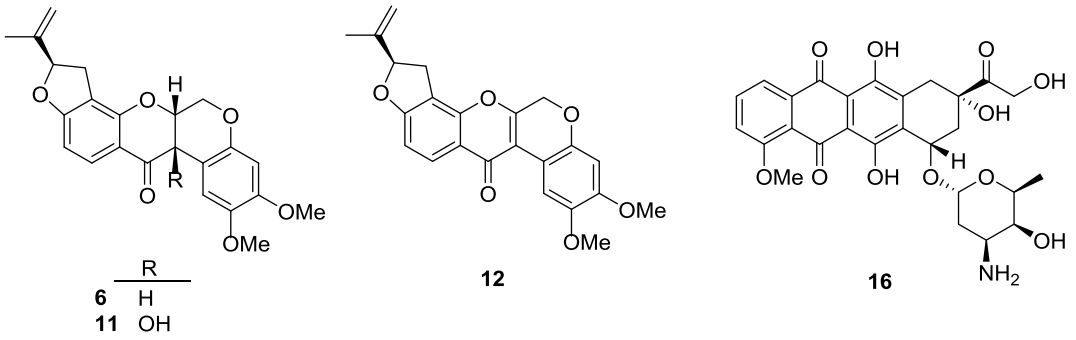

Figure 3.17 Structures of rotenoids **6**, **11** and **12** and doxorubicin (**16**)

In addition, our results indicated that the isopropenyl and gem-dimethyl moieties on E-ring are also required for their activity. Thus, compounds **4** and **5**, lacking of these functional groups, were inactive on three cancer cells tested (IC_{50} > 33 μM). Likewise, the fully fused four ring core of the rotenoid is necessary for toxicity toward cancer cells, as seen in the obtained results of compound **15**. Further, compounds **1**-**2**, **6** and **11**-**12** were tested for their toxicity on human normal colon CCD841 cells (**Table 3.5**). Only compound **11** displayed less toxicity to normal colon cells than HCT-116 colon cancer cells, by about 2 fold. Compound **11** was thus chosen for further.

Table 3.5 Cytotoxic activities of isolated rotenoids on cancer cell lines and normal cell line

Compound	IC_{50}[a] (μM)				SI[c]
	CaSki	HCT-116	Hep-G2	CCD841	
1	> 33	0.36	12.82	0.39	1.08
2	29.01	0.51	18.03	0.36	0.71
4	> 33	6.33	> 33	-[b]	-[b]
5	> 33	3.41	> 33	-[b]	-[b]
6	30.21	0.12	17.11	0.11	0.92
11	> 33	0.25	6.79	0.47	1.88
12	> 33	4.45	24.27	5.55	1.23
15	> 33	11.21	> 33	-[b]	-[b]
Doxorubicin	0.89	0.41	1.36	0.14	0.34

a: IC_{50} = 50% inhibition concentration; b: Did not determined;

c: SI = Selective index = IC_{50} of compound in CCD841/IC_{50} of the same compound in HCT-116

CaSki = human cervical carcinoma, HCT-116 = colon cancer,

Hep-G2 = hepato carcinoma, CCD841 = normal human colon epithelial

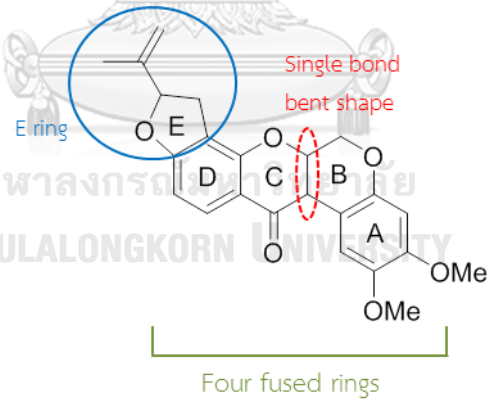

Figure 3.18 Functional groups required for cytotoxicity of rotenoid

3.4 Wound-healing activity

Tumor metastasis is a process of dissemination of primary tumors to secondary sites through blood/lymphatic vessels, which is a complex process involving several steps [27]. One of the most critical steps is cancer migration, which

is recognized as an important prerequisite process necessary for successful metastasis. A growing of in vivo evidence has revealed that the inhibition of cancer cell mobility could lead to the suppression in metastasis [28, 29]. Therefore the attenuation of the cancer migration is a clinically effective therapeutic approach towards cancer. To investigate the effect of rotenoid **11** on HCT-116 cell migration, wound-healing assay was performed with keratinocyte monolayer in which a gap in the cell layer was created by a microtip scratch. Cells were treated with various concentrations of **11** (0-1 μM) for 24 h, and the migratory behavior was observed under microscope and a gap closure was determined. The results showed that the vehicle control groups migrate more than half to fill in the initial wound space after 24 h, whereas treatment with **11** significantly suppressed cell migration in a dose-dependent manner (**Figure 3.19**). Approximately 25, 90 and 98% reductions in cell mobility were observed in cells treated with 0.25, 0.5 and 1 μM, respectively. Based on the above results, it indicated that rotenoid **11** potently inhibited the HCT-116 cell migration.

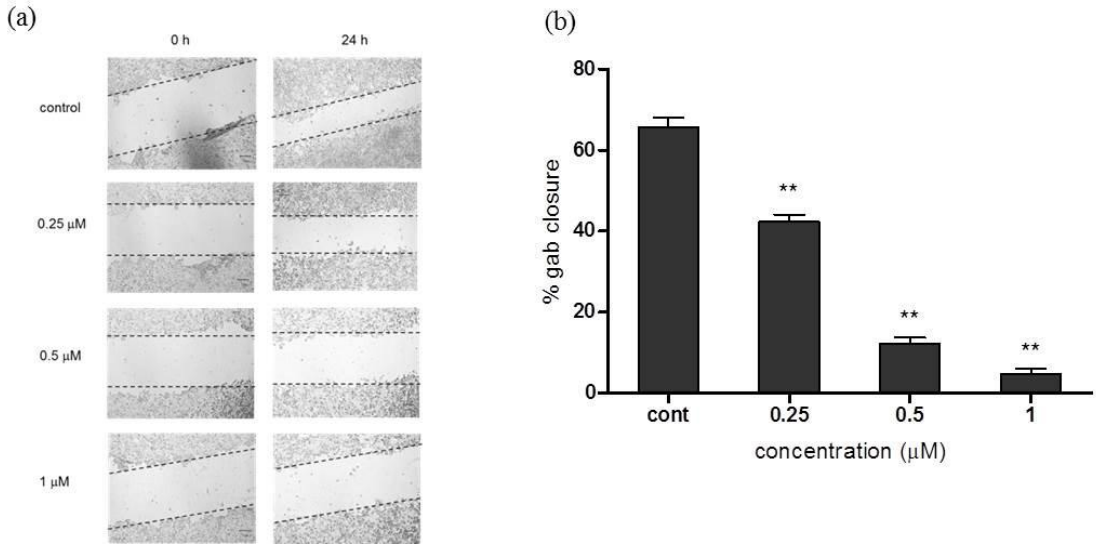

Figure 3.19 Effect of 12a-hydroxyrotenone (**11**) on human colon cancer HCT-116 cell migration. (a) A confluent monolayer of HCT-116 was wounded using a 1 mm width tip incubated with various doses of 2 (0-1 μM) at 0 and 24 h. (b) % Gab closure of HCT-116 after treatment for 24 h was determined. Data are expressed as mean ± SEM (n = 3), ** $p < 0.05$, * $p < 0.05$ vs. control.

3.5 Anti-angiogenic activity

Angiogenesis involving in the formation of new blood vessels from the pre-existing ones plays a pivotal role in the process of cancer growth and metastasis, blocking angiogenesis is one of the validated effective approaches against cancer [27]. To determine the effect of the isolated compounds on angiogenic inhibition, the compounds were subjected to an ex vivo model to monitor their suppressing potential on microvessel sprouting from a rat aortic ring. Their effect at two doses, 1 and 10 μM, was first examined to identify the most potent compound and to look at their structure-activity relationship (**Figure 3.20**).

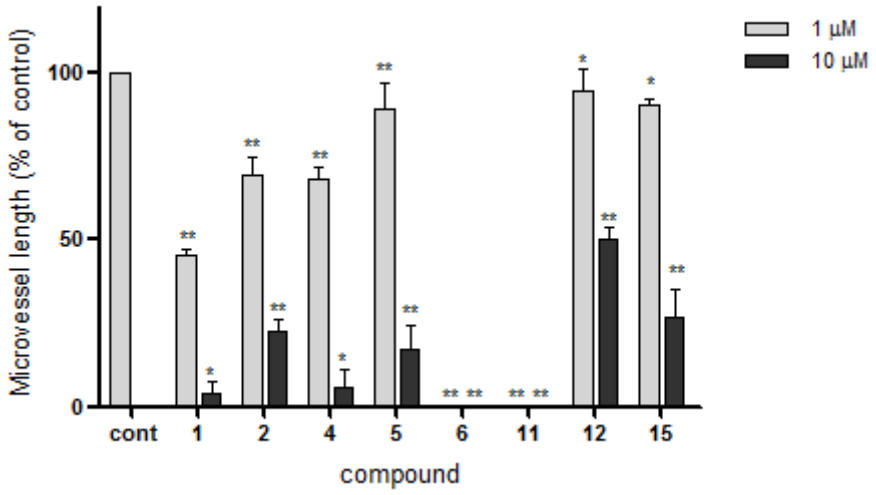

Figure 3.20 Anti-angiogenic activity of isolated rotenoids in ex vivo assay. Effects were assessed by measuring the microvessel length from rat aortic at two concentrations of sample treatment, 1 and 10 μM, as compared to that of the control. Data are expressed as mean ± SEM (n = 6), ** $p < 0.05$, * $p < 0.05$ VS control.

Results showed that rotenoids **6** and **11** exhibited the strongest anti-angiogenic activity with the completion of the suppressing microvessel sprouting at only 1 μM, while the existence of a C-6a–C-12a double bond in compound **12** caused almost loss in a whole activity at this concentration. It was supposed that this might be because of the molecular shape of the rotenoids as found in cytotoxic

results. Among the remaining rotenoids with a fully fused four ring, compound **1** showed the potent activity at ~95% and ~50% inhibition at doses of 10 and 1 μM, respectively, while compounds **2** and **4**-**5** were all less active. Similar to cytotoxicity, the fully fused four ring of the rotenoid is required for angiogenesis inhibition, since there was only a slight inhibition by compound **15**.

Based on the results obtained from the screening using ex vivo model, only compounds **6** and **11** were subjected to further evaluation, starting with its potency to suppress microvessel outgrowth by treating aortic rings with various doses of the compounds. As shown in **Figure 3.21**, the inhibitory effect of both compounds was in a dose-dependent manner. However, compound **11** displayed more potent anti-angiogenic activity than **6**, because there was no apparent significant suppression of microvessel sprouting by **6** at 0.1 μM, while rotenoid **11** still provided ~40% inhibition at the same concentration.

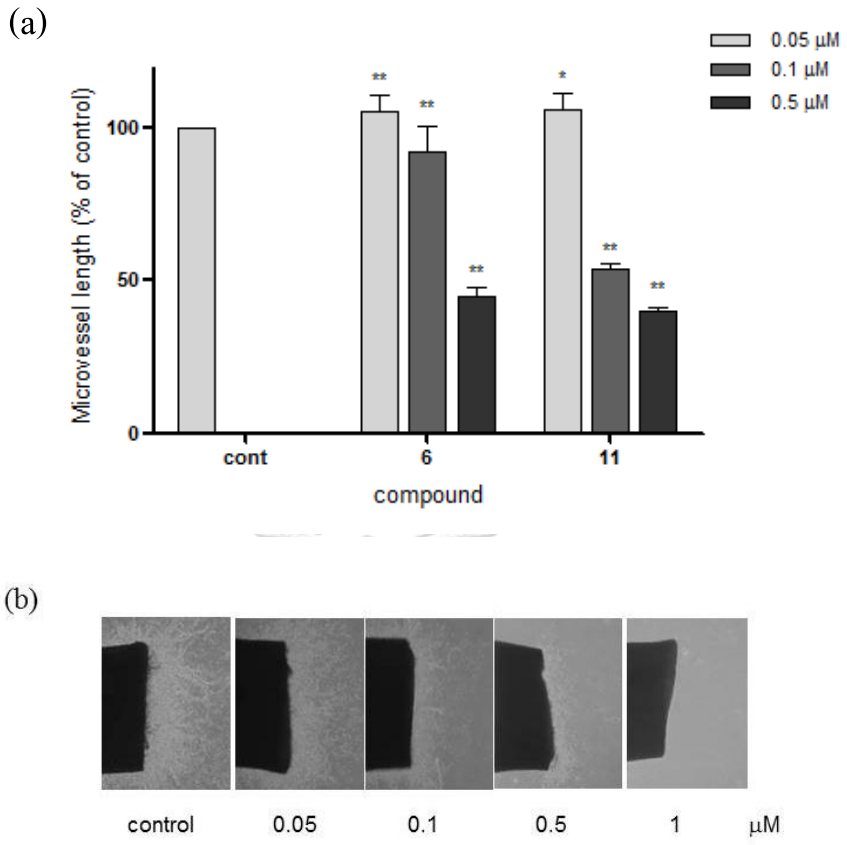

Figure 3.21 Anti-angiogenic activity of rotenone (**1**) and 12a-hydroxyrotenone (**11**) at various concentrations in ex vivo assay. (b) Representative photographs of microvessel sprout grown from aortic rings when treated with **11** at various doses. Effects were assessed by measuring the microvessel length from rat aortic at various doses of compounds, compared to that of the control. Data are expressed as mean ± SEM (n = 6), ** $p < 0.05$, * $p < 0.05$ VS control.

Endothelial cells (ECs), a specialized type of epithelial cell forming the inner layer of blood vessels, play a central role in angiogenesis. During angiogenic process, they are activated and express matrix metalloproteinases (MMPs) which lead to the degradation of the basal membrane of the parent vessel and of the extra-cellular surrounding matrix. In response to environmental cues, ECs secrete MMPs and subsequently invade through the basement membrane to form new microvessel networks [30]. Human umbilical vein endothelial cells (HUVECs) are most commonly

used human EC type for angiogenesis study. To examine how rotenoid **11** could exert the anti-angiogenic effect, it is in vitro inhibitory activity towards the functions of HUVECs was evaluated in term of ECs proliferation, tube formation and migration.

Since activation of ECs proliferation is one of the common features of angiogenesis, inhibition of their proliferation is one strategy for anti-angiogenesis [31]. Thus the effect of **11** on HUVECs proliferation was first investigated by using the WST-8 assay. As shown in **Figure 3.22**, 12a-hydroxyrotenone (**11**) could inhibit HUVECs proliferation in a dose-dependent manner with an IC_{50} value as little as 0.0127 μM.

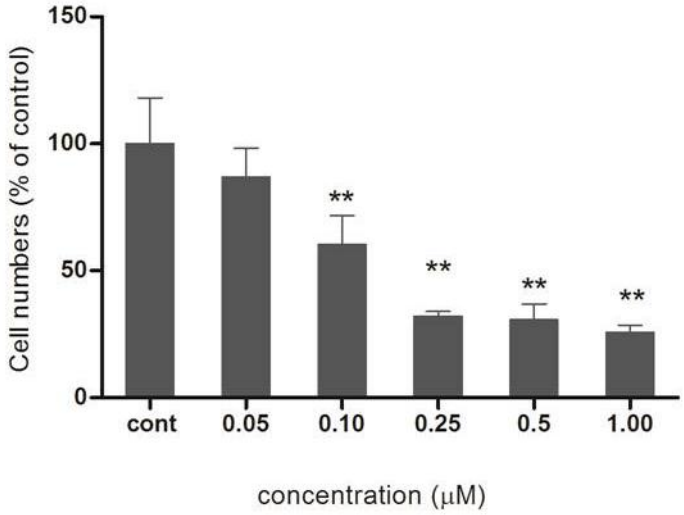

Figure 3.22 Effect of 12a-hydrorotenone (**11**) on HUVECs proliferation function. Data are expressed as mean ± SEM (n = 6), ** $p < 0.05$, * $p < 0.05$ vs. control.

To further assess the effect of **11** on angiogenesis, whether it could regulate capillary tube formation of ECs by seeding HUVECs onto two-dimensional Matrigel matrix and then allowing them to migrate, attach to each other and form tubular-like structures [32]. The effect of the compound was evaluated by measuring the length of tubular-structured cells compared to the vehicle control after treatment for 12 h. HUVECs showed robust capillary network for control, whereas compound **11** was found to inhibit tube formation in the ECs in a dose-dependent manner with a significant inhibition being observed at 0.25 μM and an IC_{50} value of 0.27 μM (**Figure 3.23**).

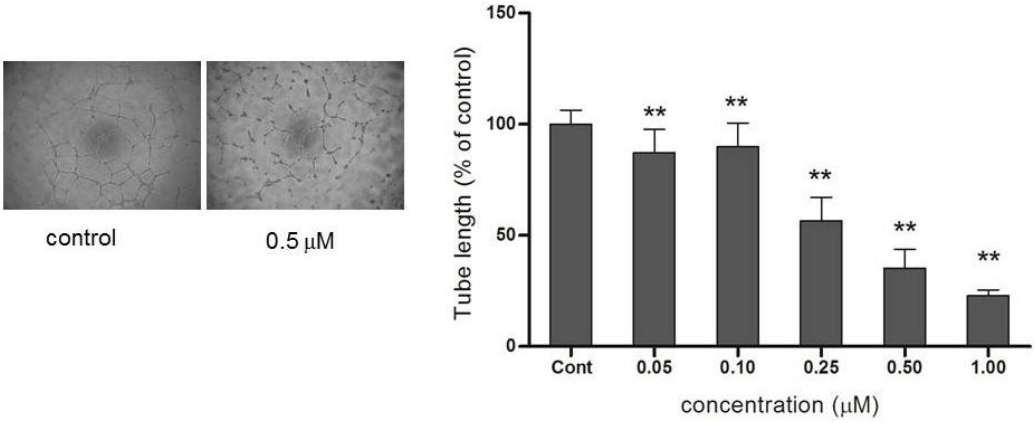

Figure 3.23 Effect of 12a-hydrorotenone (**11**) on HUVECs tube formation function. Data are expressed as mean ± SEM (n = 6), ** $p < 0.05$, * $p < 0.05$ vs. control.

Finally, the effect of **11** on the VEGF-induced migration of HUVECs was examined using a Boyden chamber assay. VEGF is known as a specific and key growth factor involved in ECs proliferation, migration and survival during blood vessel formation [33]. As shown in **Figure 3.24**, VEGF strongly stimulated HUVECs migration; however, compound **11** did not show any detectable effect upon this, suggesting that **11** might not be involved in VEGF-induced ECs migration.

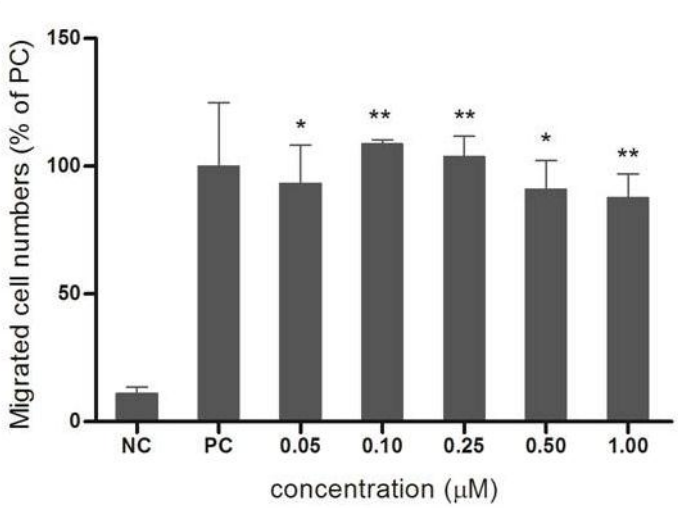

Figure 3.24 Effects of 12a-hydroxyrotenone (**11**) on HUVECs chemotactic migration functions. Data are expressed as mean ± SEM (n = 6), ** $p < 0.05$, * $p < 0.05$ vs. control.

Taken together, the results indicated that the anti-angiogenic activity by compound **11** was mainly the inhibition of ECs proliferation and tube formation, not involved in ECs migration.

CHAPTER IV
CONCLUSION

In conclusion, purification of the EtOAc extract of *D. trifoliata* stem led to the isolation of eight rotenoids, deguelin (**1**), tephrosin (**2**), elliptone (**4**), 12a-hydroxyelliptone (**5**), rotenone (**6**), 12a-hydroxyrotenone (**11**), 6a, 12a-dehydrorotenone (**12**) and 7a-*O*-methylelliptonal (**15**).

The effect of isolated rotenoids on cytotoxicity against cancer cell lines and anti-angiogenic activity was determined. Based on the results from both assays, it could be concluded that a fully fused four ring skeleton, a bent-shape conformation between C-6a and C-12a, and isopropenyl moiety on E-ring is required for cytotoxic and anti-angiogenic activities of rotenoids. Moreover, it was found that 12a-hydroxyrotenone (**11**) could potently inhibit cell growth (IC_{50} 0.25 μM) and migration of colon cancer HCT-116 cells (>90% inhibition at 0.5 μM). Furthermore, results from both ex vivo and in vitro anti-angiogenic assays have indicated that rotenoid **11** was a promising anti-angiogenic agent and it mainly functions by suppression of endothelial cells proliferation and tube formation, but has no effect of ECs migration at all.

Together, the present study demonstrated that compound **11** may be suitable for using as a lead compound or for further development to overcome cancer metastasis.

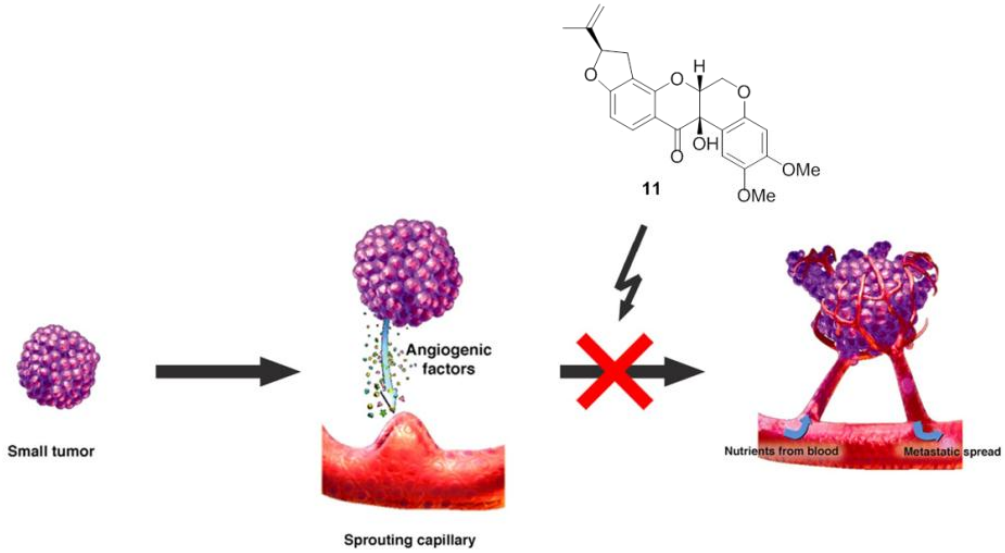

Figure 4.1 Tumor expansion induced by the sprouting of blood vessels [34]

REFERENCES

1. Rahul Kumar, et al., *CancerDR: Cancer Drug Resistance Database.* SCIENTIFIC REPORTS, 2013.
2. Peter Carmeliet and R.K. Jain, *Angiogenesis in cancer and other diseases.* Nature, 2000. **407**: p. 249-257.
3. Bergers, G. and L.E. Benjamin, *Tumorigenesis and the angiogenic switch.* Nat Rev Cancer, 2003. **3**(6): p. 401-10.
4. Judah Folkman and Y. Shing, *Angiogenesis.* Biological Chemistry, 1992. **267**: p. 10931-10934.
5. Judah Folkman and M.D., *Angiogenesis inhibitors generated by tumors.* Molecular Medicine, 1995. **1**: p. 120-122.
6. Johnson, T.A., et al., *Natural product libraries to accelerate the high-throughput discovery of therapeutic leads.* J Nat Prod, 2011. **74**(12): p. 2545-55.
7. Rodney Croteau, T.M.K., Norman G. Lewis, *Biochemistry & Molecular Biology of Plants.* American Society of Plant Physiologists, 2000.
8. Cragg, G.M. and D.J. Newman, *Natural products: a continuing source of novel drug leads.* Biochim Biophys Acta, 2013. **1830**(6): p. 3670-95.
9. Bingham, K.K.a.B.L., *Biology of mangroves and mangrove Ecosystems.* Advances in Marine Biology, 2001. **40**: p. 81-251.
10. 2017; Available from: http://lkcnhm.nus.edu.sg/dna/organisms/details/483.
11. *Australian Tropical Rainforest Plants*. 2010 December 2010; Available from: http://keys.trin.org.au/key-server/data/0e0f0504-0103-430d-8004-060d07080d04/media/Html/taxon/Derris_trifoliata.htm
12. Nianbai Fang and J.E. Casida, *Cube´ Resin Insecticide: Identification and Biological Activity of 29 Rotenoid Constituents.* J. Agric. Food Chem., 1999. **47**: p. 2130-2136.
13. Deyou T, G.I., Pang F, Gruhonjic A, Mumo M, Holleran J, Duffy S, Fitzpatrick PA, Heydenreich M, Landberg G, Derese S, Avery V, Rissanen K, Erdelyi M,

Yenesew A., *Rotenoids, flavonoids, and chalcones from the root bark of Millettia usaramensis.* J Nat Prod, 2015. **78**: p. 2932–2939.

14. Tewtrakul, S., S. Cheenpracha, and C. Karalai, *Nitric oxide inhibitory principles from Derris trifoliata stems.* Phytomedicine, 2009. **16**(6-7): p. 568-72.
15. Yenesew, A., et al., *Two unusual rotenoid derivatives, 7a-O-methyl-12a-hydroxydeguelol and spiro-13-homo-13-oxaelliptone, from the seeds of Derris trifoliata.* Phytochemistry, 2006. **67**(10): p. 988-91.
16. Ito, C., et al., *Cancer chemopreventive activity of rotenoids from Derris trifoliata.* Planta Med, 2004. **70**(1): p. 8-11.
17. Jeong Hun Kim, J.H.K., Young Suk Yu, Kyu Hyung Park, Hye Jin Kang, Ho-Young Lee, and Kyu-Won Kim, *Antiangiogenic Effect of Deguelin on Choroidal Neovascularization.* THE JOURNAL OF PHARMACOLOGY AND EXPERIMENTAL THERAPEUTICS, 2007. **324**: p. 643-647.
18. Pompeng, P., et al., *Antiangiogenetic effects of anthranoids from Alternaria sp., an endophytic fungus in a Thai medicinal plant Erythrina variegata.* Phytomedicine, 2013. **20**(10): p. 918-22.
19. Denis Gerlier and N. Thomasset, *Use of MTT colorimetric assay to measure cell activation.* Journal of Immunological Methods, 1986. **94**: p. 57-63.
20. Amen, Y.M., et al., *New cytotoxic lanostanoid triterpenes from Ganoderma lingzhi.* Phytochemistry Letters, 2016. **17**: p. 64-70.
21. Jackson Nunes e Vasconcelos, et al., *ROTENOIDS FROM Tephrosia toxicaria WITH LARVICIDAL ACTIVITY AGAINST Aedes aegypti, THE MAIN VECTOR OF DENGUE FEVER.* Quim. Nova, 2012. **35**: p. 1097-1100.
22. Francois Ngandeu, et al., *Rotenoid derivatives and other constituents of the twigs of Millettia duchesnei.* Phytochemistry, 2008. **69**: p. 258-263.
23. Aderbal F. Magalhaes, et al., *Twenty-three flavonoids from Lonchocarpus subglaucescens.* Phytochemistry, 1996. **42**: p. 1459-1471.
24. Arriaga, A.M., et al., *Unequivocal assignments of flavonoids from Tephrosia sp. (Fabaceae).* Magn Reson Chem, 2009. **47**(6): p. 537-40.

25. Sarot Cheenpracha, C.K., Chanita Ponglimanont, and Kan Chantrapromma, *Cytotoxic rotenoloids from the stems of Derris trifoliata.* Can. J. Chem., 2007. **85**: p. 1019–1022.

26. Chimsook, N.P.a.T., *The Structure Activity Relationship and Cytotoxicity between Stemonal and 6-Deoxyclitoriacetal.* Advanced Materials Research, 2013. **699**: p. 698-702.

27. Guan, X., *Cancer metastases: challenges and opportunities.* Acta Pharmaceutica Sinica B, 2015. **5**(5): p. 402-418.

28. Yuanzhang Fang, Y.C., Linxi Yu, Cong Zheng, Ya Qi, Zhenxi Li, Zhengfeng Yang, Yong Zhang, Tieliu Shi, Jian Luo and Mingyao Liu, *Inhibition of Breast Cancer Metastases by a Novel Inhibitor of TGFβ Receptor 1.* Journal of the National Cancer Institute, 2012. **105**(1): p. 47-58.

29. Pienta KJ, N.H., Akhtar A, Yamazaki K, Replogle TS, Lehr J, Donat TL, Tait L, Hogan V, Raz A., *Inhibition of spontaneous metastasis in a rat prostate cancer model by oral administration of modified citrus pectin.* J Natl Cancer Inst., 1995. **87**: p. 348-353.

30. Shinkaruk S., B.M., Laïn G., Déléris G., *Vascular endothelial cell growth factor (VEGF), an emerging target for cancer chemotherapy.* Curr Med Chem Anticancer Agents., 2003. **3**(2): p. 95-117.

31. Feng J, Z.X., Xing, D., *Low-power laser irradiation (LPLI) promotes VEGF expression and vascular endothelial cell proliferation through the activation of ERK/Sp1 pathway.* Cell Signal, 2012. **14**: p. 1116-1125.

32. Kayashima T, M.M., Yoshida H, Mizushina Y, Matsubara K., *1,4-Naphthoquinone is a potent inhibitor of human cancer cell growth and angiogenesis.* Cancer Letters, 2009. **278**: p. 34-40.

33. Ferrrara, N., *Vascular endothelial growth factor: molecular and biological aspects.* Curr. Top. Microbiol. Immunol., 1999. **237**: p. 1-30.

34. Vera Loizzi , V.D.V., Giulio Gargano, Maria De Liso, Anila Kardashi, Emanuele Naglieri, Leonardo Resta, Ettore Cicinelli and Gennaro Cormio, *Biological Pathways Involved in Tumor Angiogenesis and Bevacizumab Based Anti-*

Angiogenic Therapy with Special References to Ovarian Cancer. International Journal of Molecular Sciences, 2017. **18**: p. 1-11.

APPENDIX

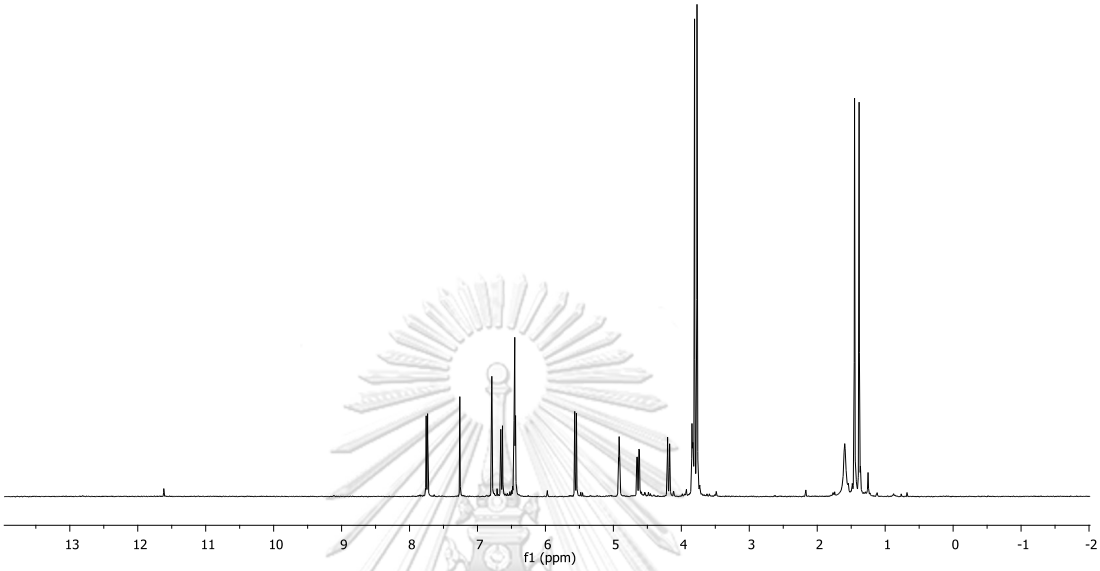

Figure A.1 ^{1}H NMR (400 MHz, $CDCl_3$) spectrum of compound **1**

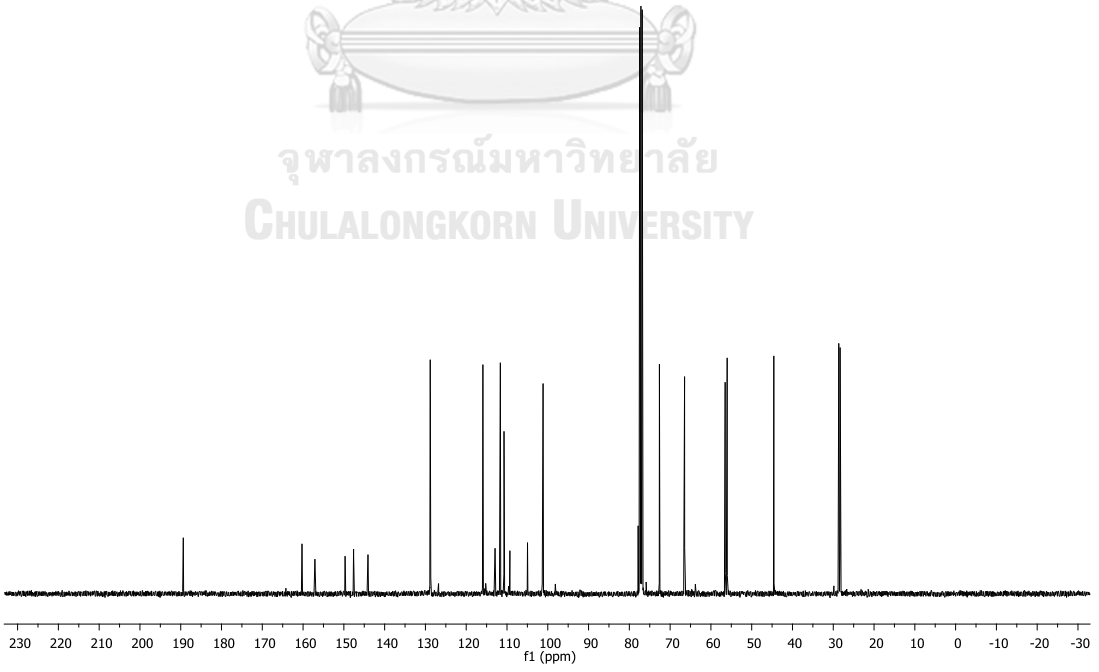

Figure A.2 ^{13}C NMR (100 MHz, $CDCl_3$) spectrum of compound **1**

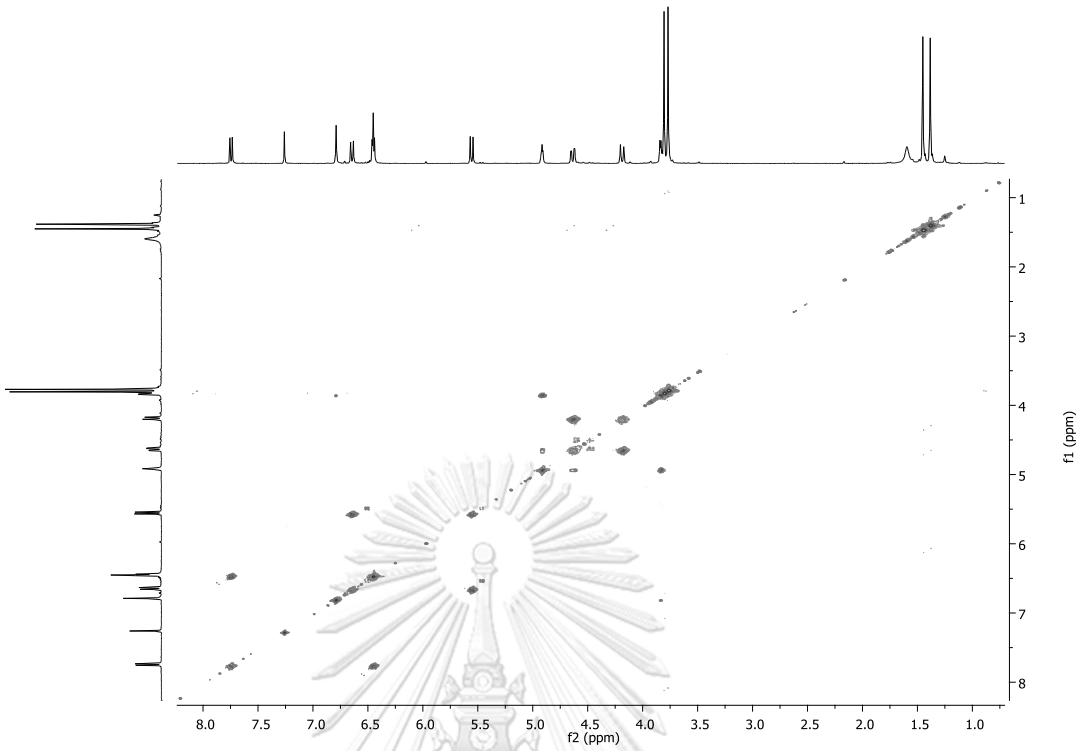

Figure A.3 ^{1}H-^{1}H COSY spectrum ($CDCl_3$) of compound **1**

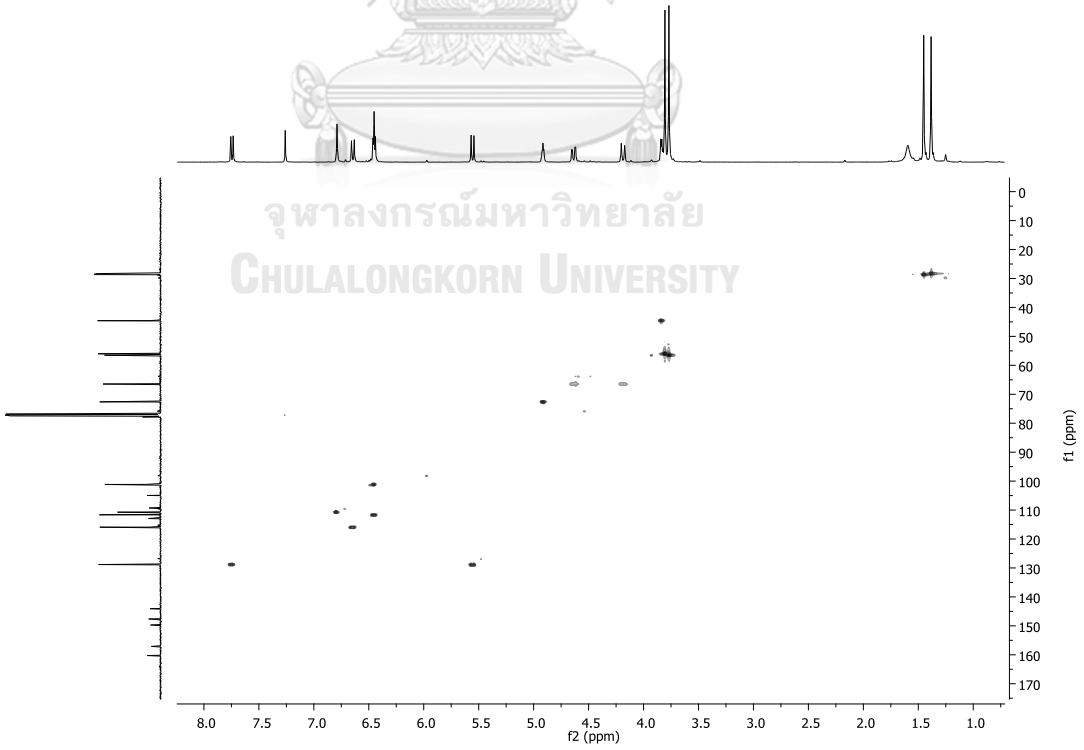

Figure A.4 HSQC spectrum ($CDCl_3$) of compound **1**

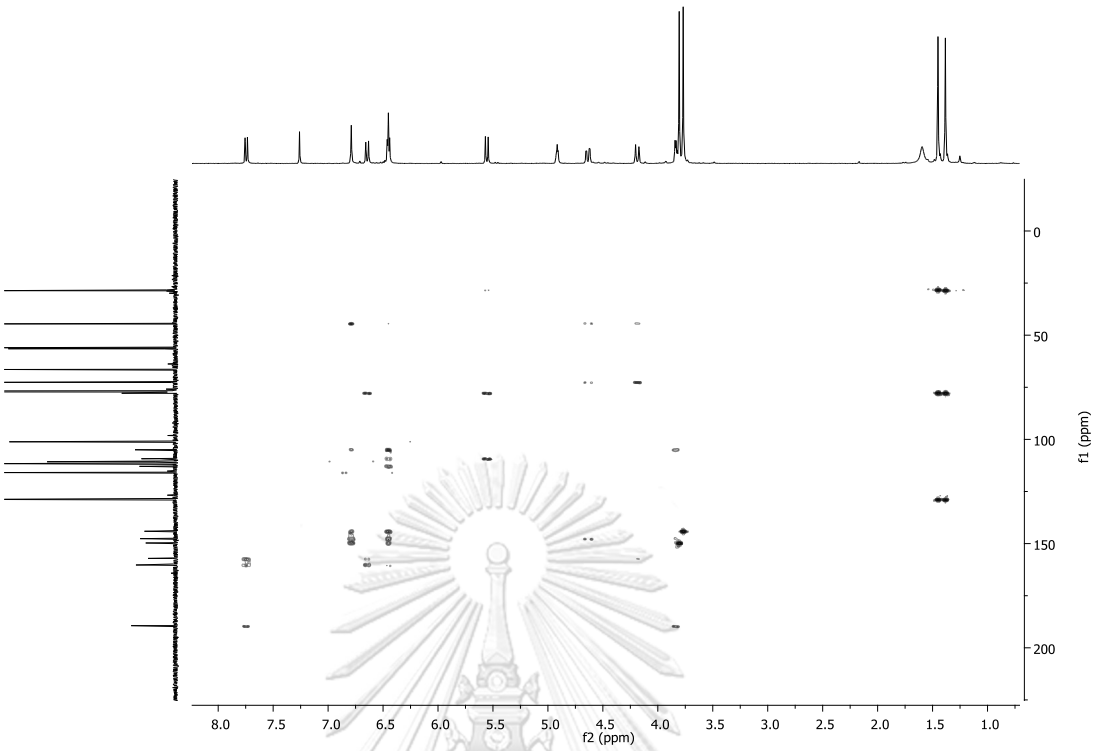

Figure A.5 HMBC spectrum ($CDCl_3$) of compound **1**

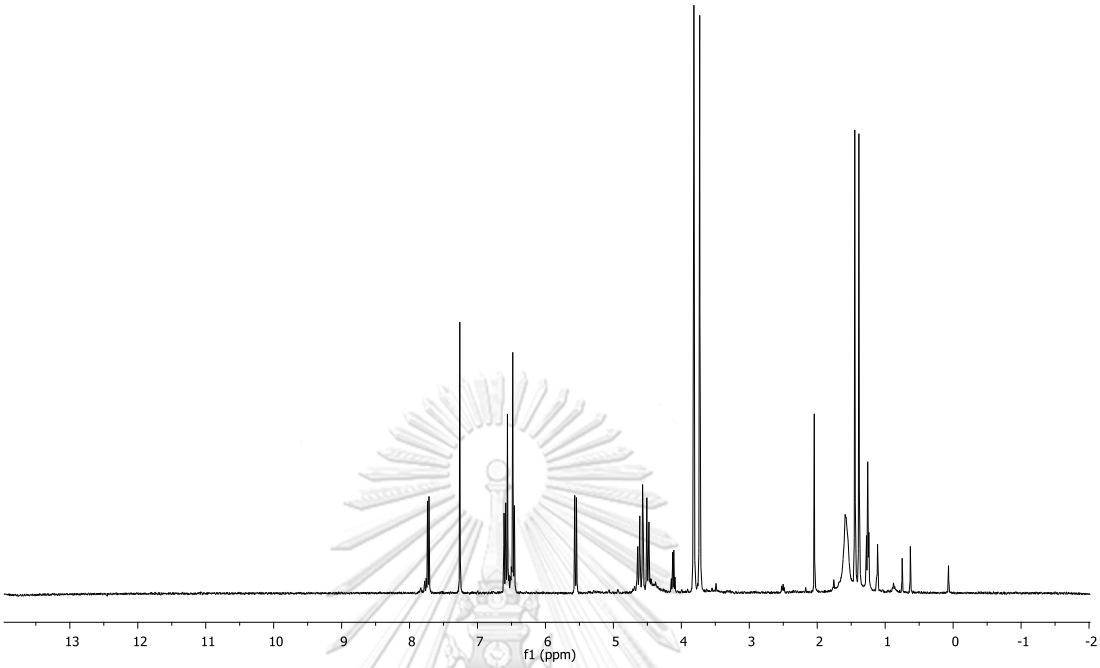

Figure A.6 ^{1}H NMR (400 MHz, $CDCl_3$) spectrum of compound **2**

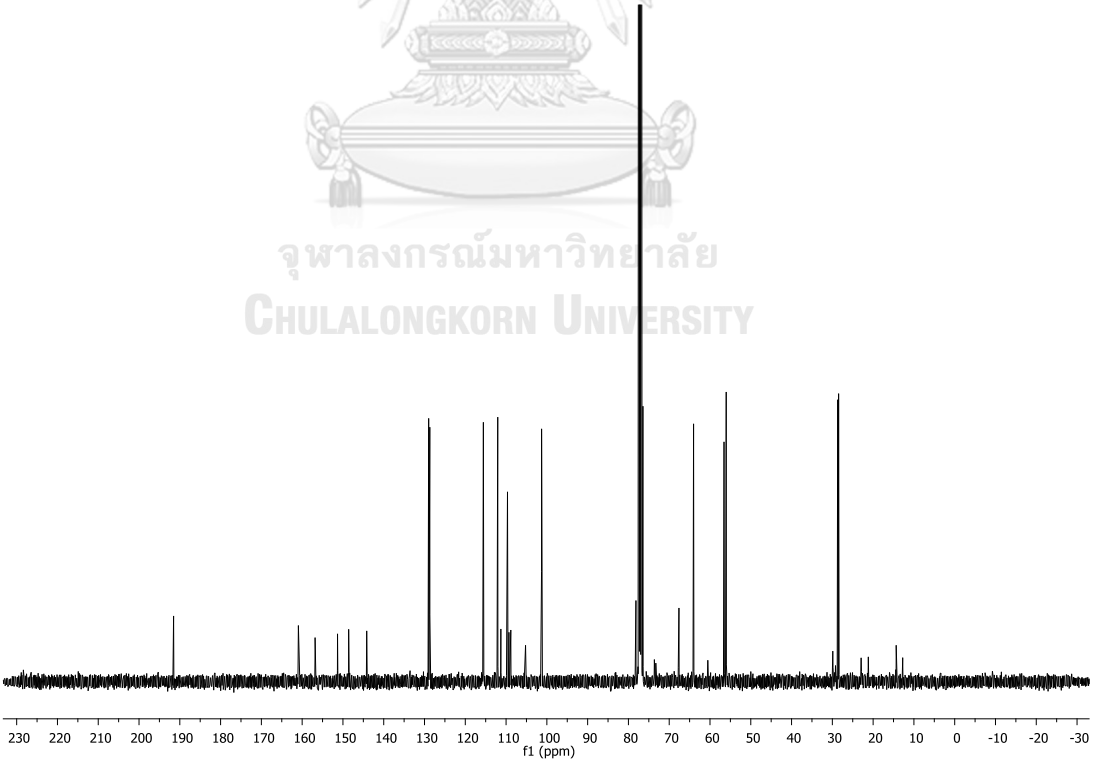

Figure A.7 ^{13}C NMR (100 MHz, $CDCl_3$) spectrum of compound **2**

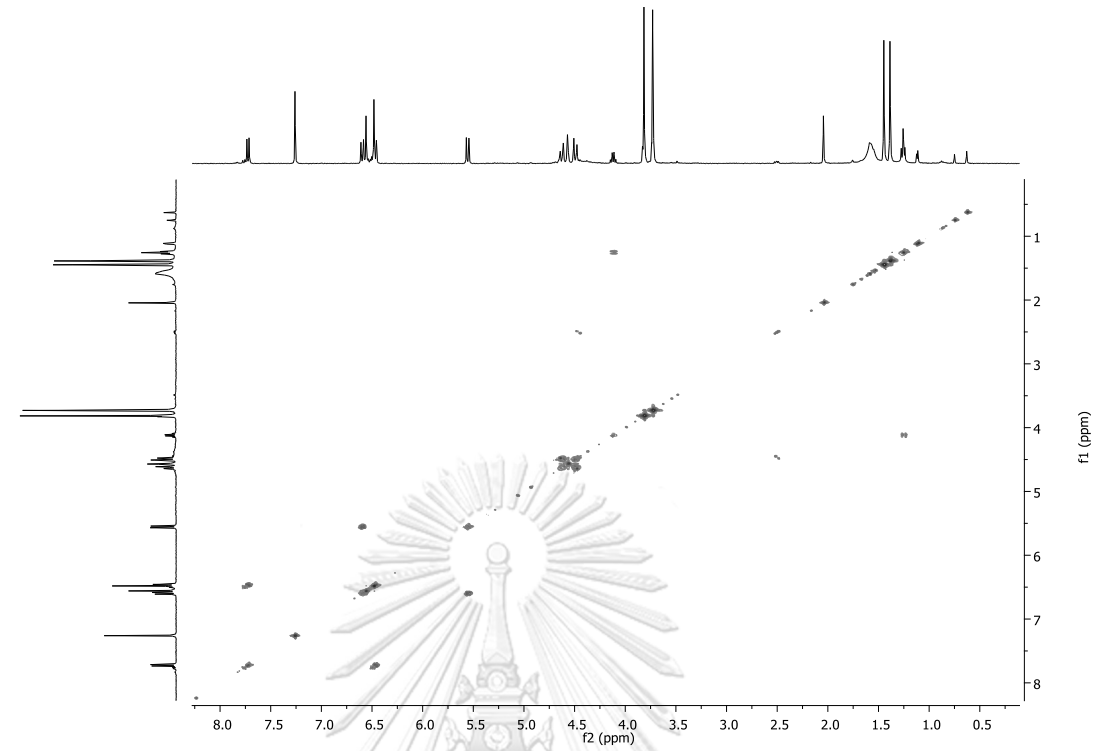

Figure A.8 ^{1}H-^{1}H COSY spectrum ($CDCl_3$) of compound **2**

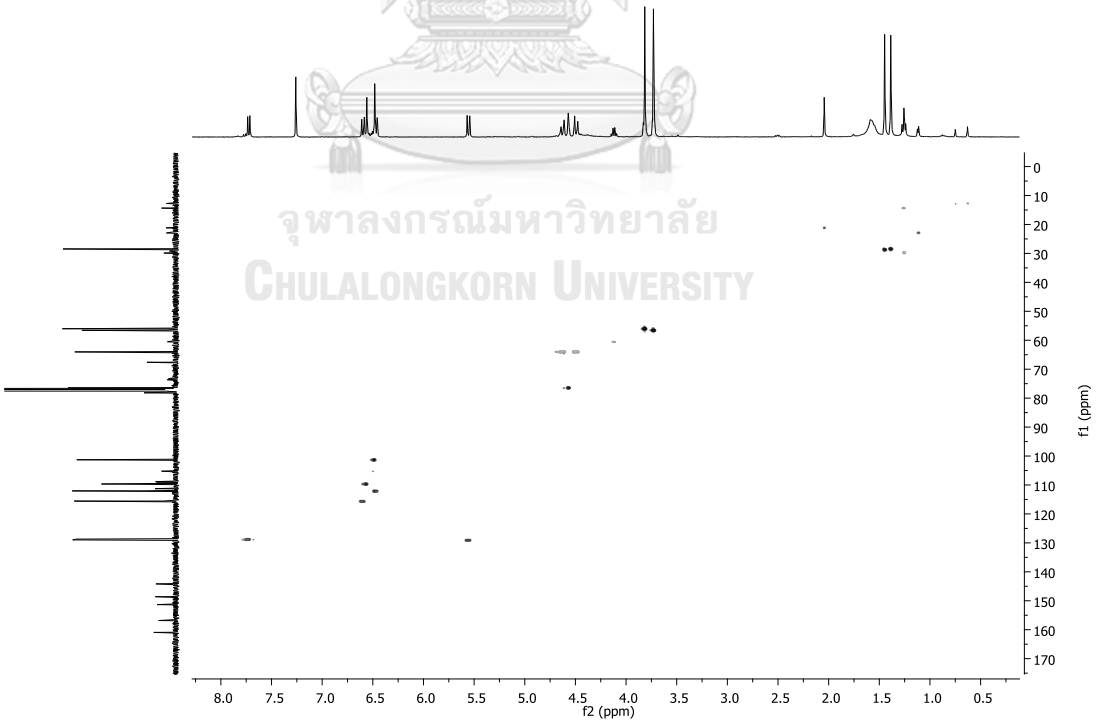

Figure A.9 HSQC spectrum ($CDCl_3$) of compound **2**

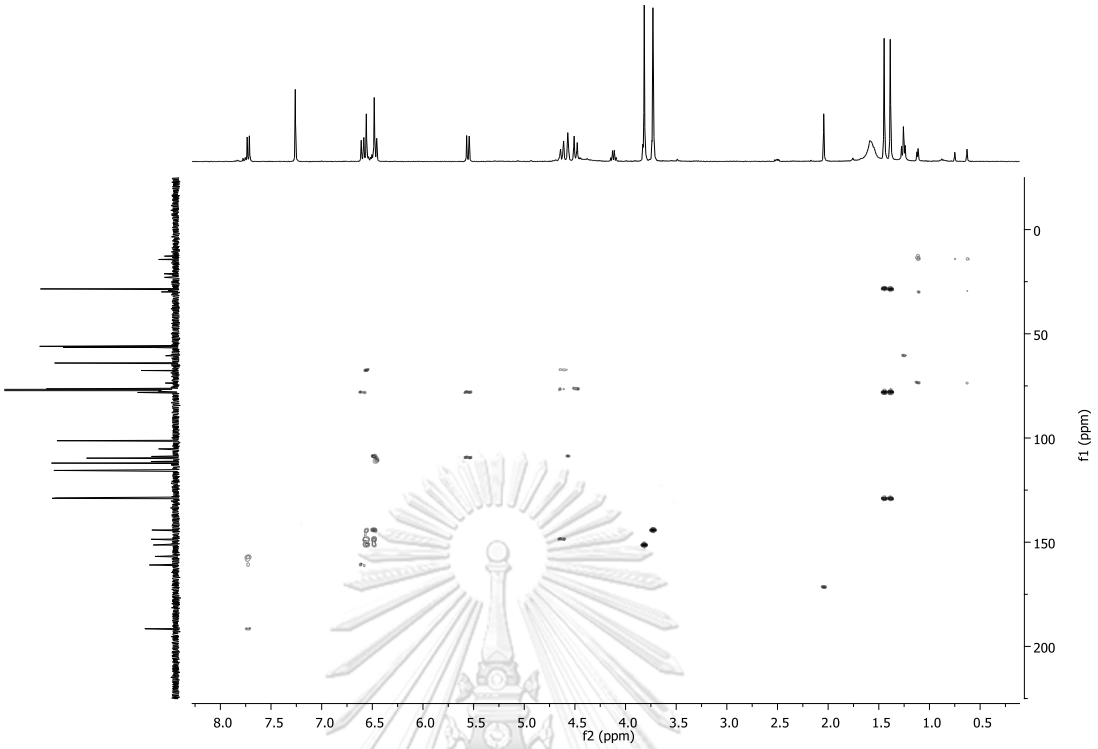

Figure A.10 HMBC spectrum ($CDCl_3$) of compound **2**

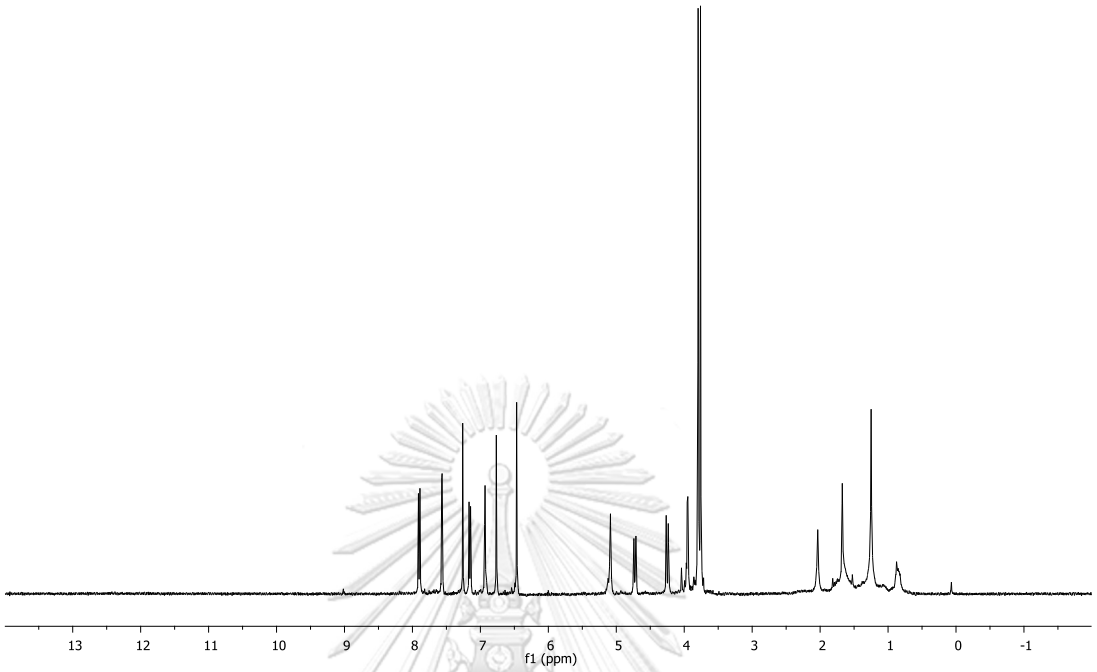

Figure A.11 ^{1}H NMR (400 MHz, $CDCl_3$) spectrum of compound **4**

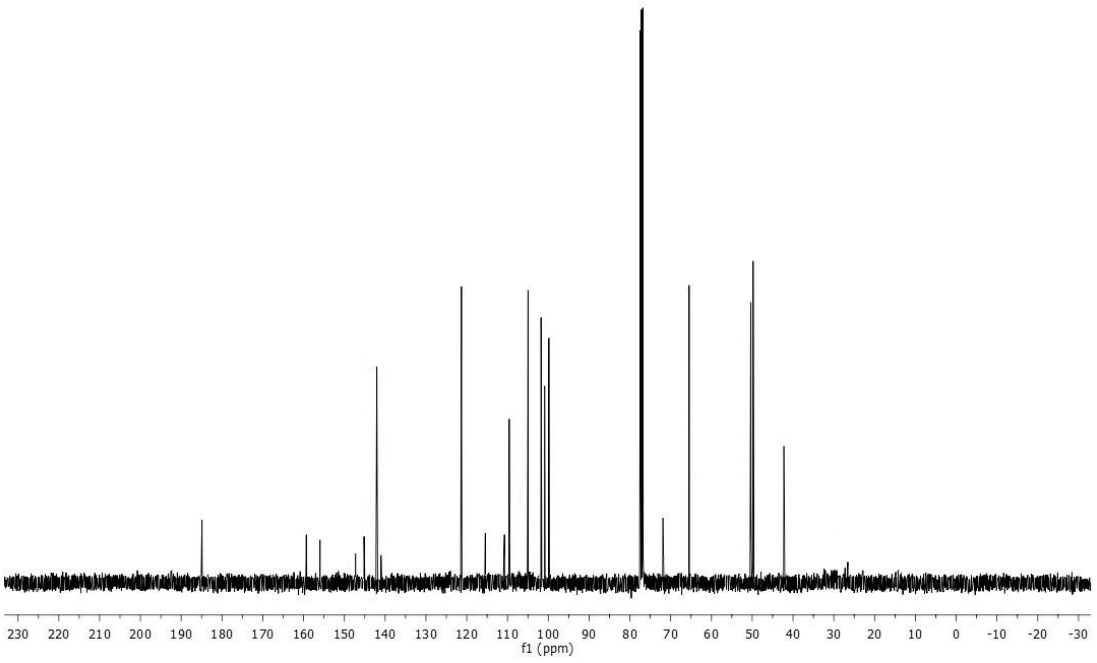

Figure A.12 ^{13}C NMR (100 MHz, $CDCl_3$) spectrum of compound **4**

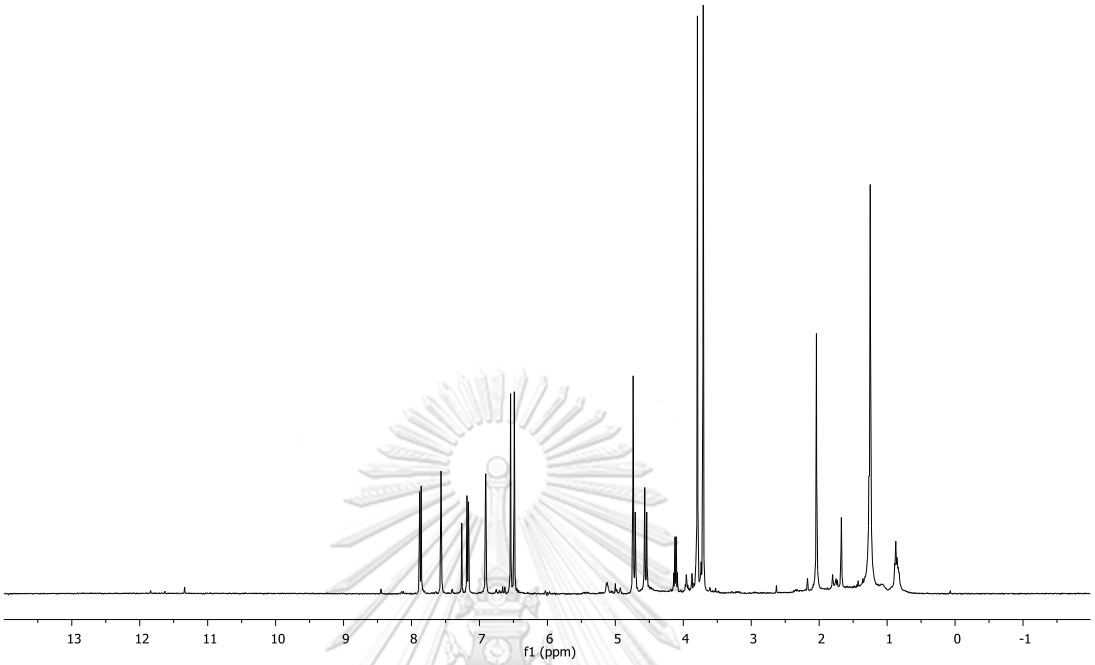

Figure A.13 ^{1}H NMR (400 MHz, $CDCl_3$) spectrum of compound **5**

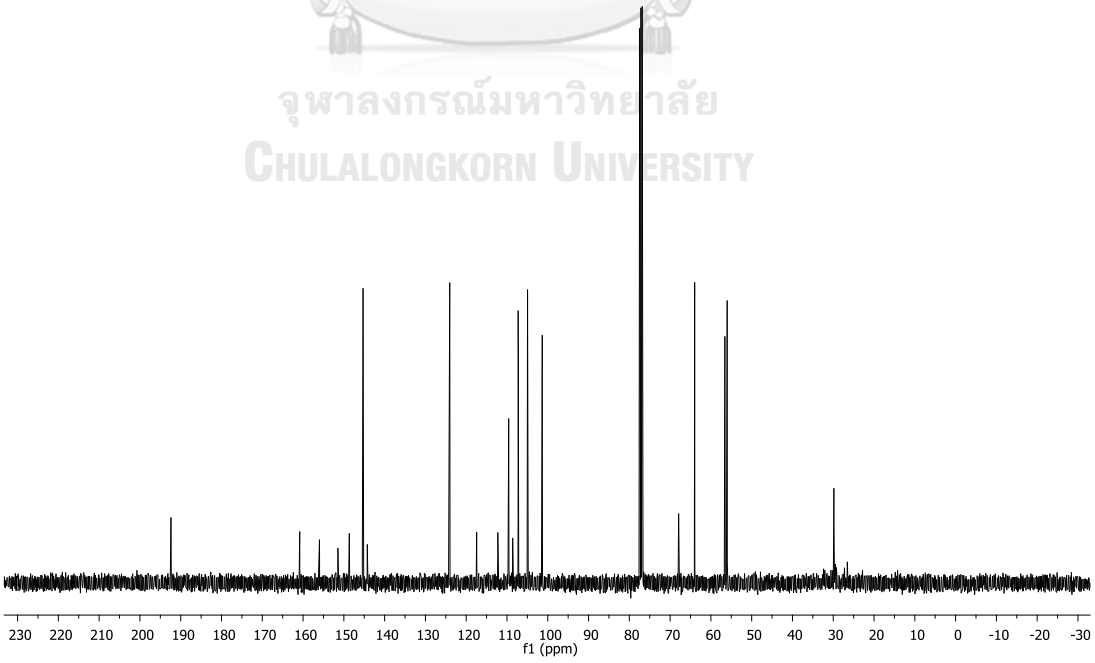

Figure A.14 ^{13}C NMR (100 MHz, $CDCl_3$) spectrum of compound **5**

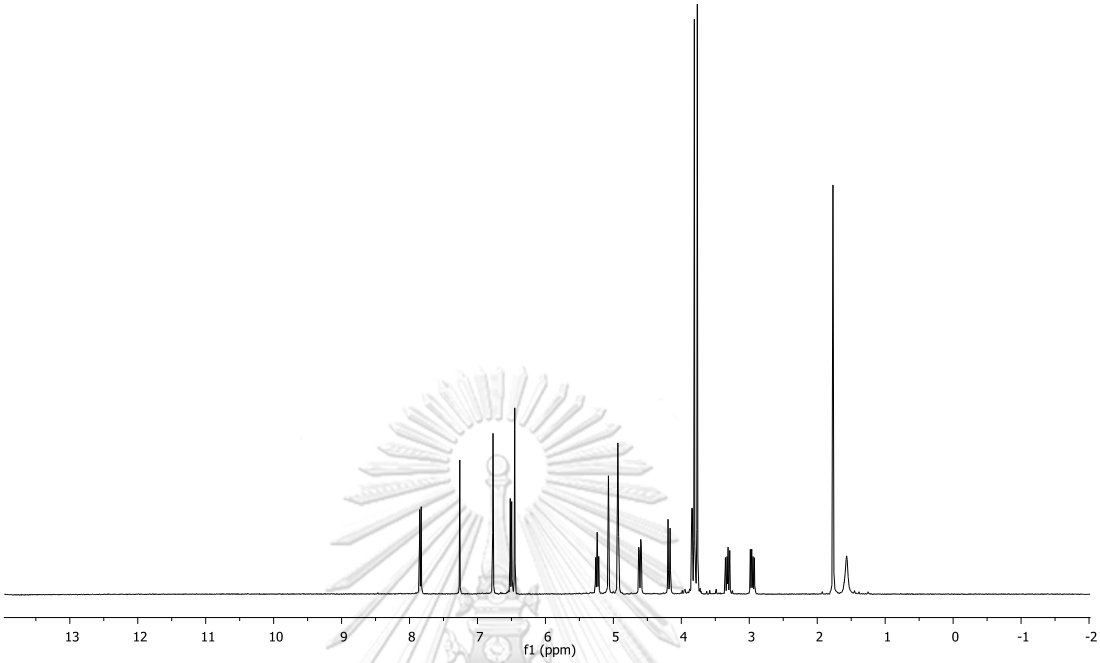

Figure A.15 ^{1}H NMR (400 MHz, $CDCl_3$) spectrum of compound **6**

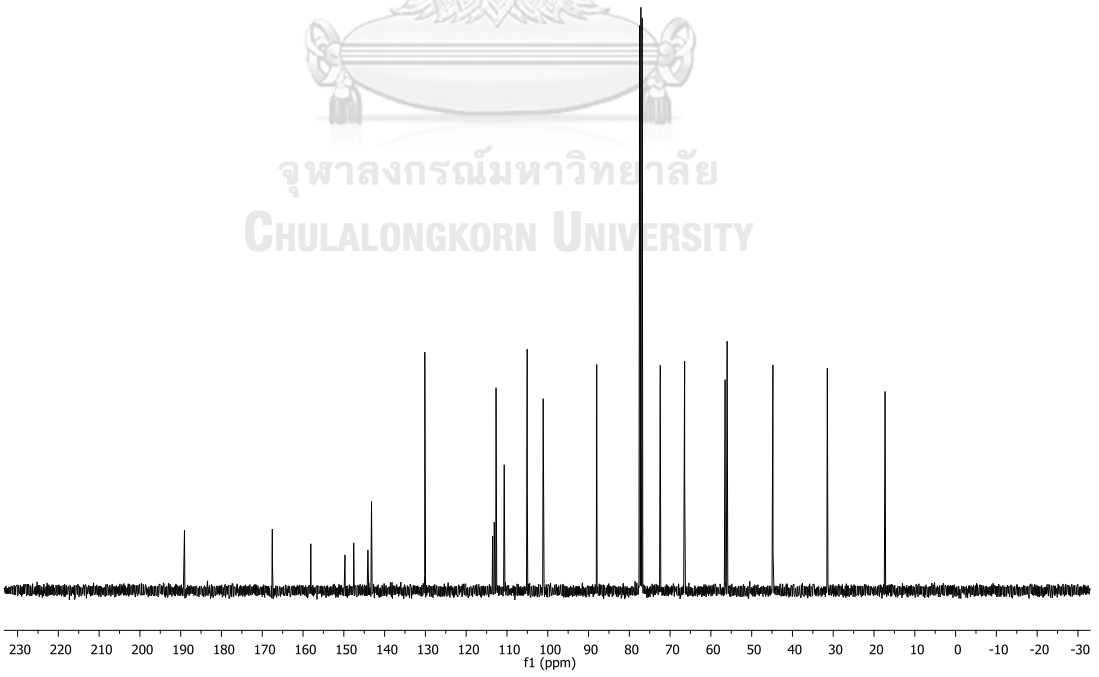

Figure A.16 ^{13}C NMR (100 MHz, $CDCl_3$) spectrum of compound **6**

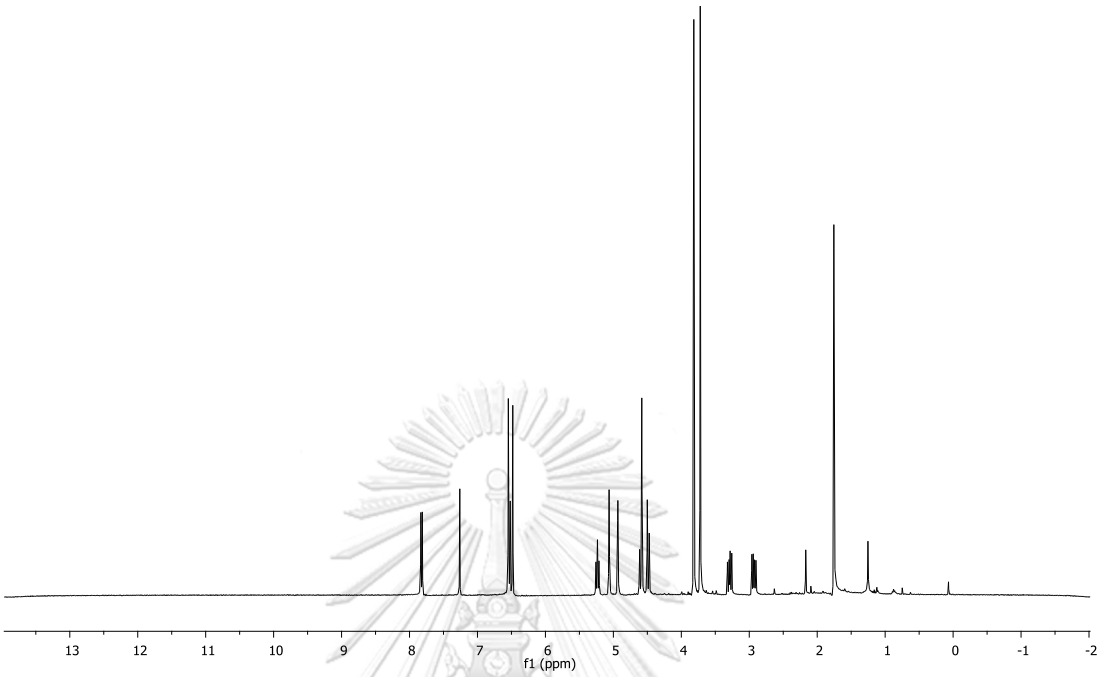

Figure A.17 ^{1}H NMR (400 MHz, $CDCl_3$) spectrum of compound **11**

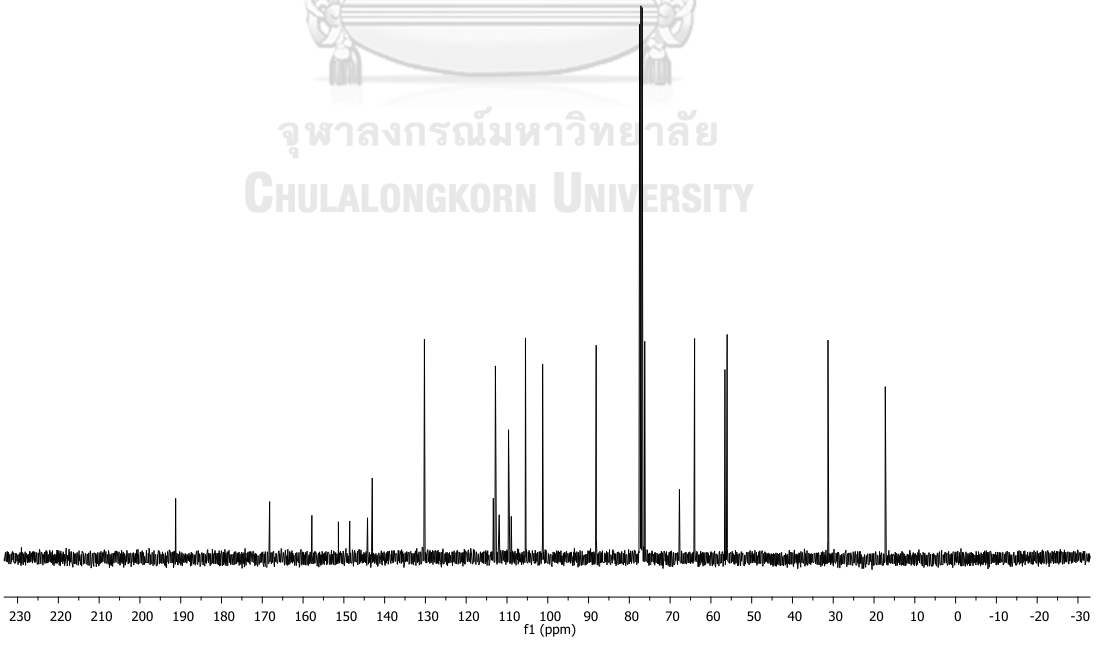

Figure A.18 ^{13}C NMR (100 MHz, $CDCl_3$) spectrum of compound **11**

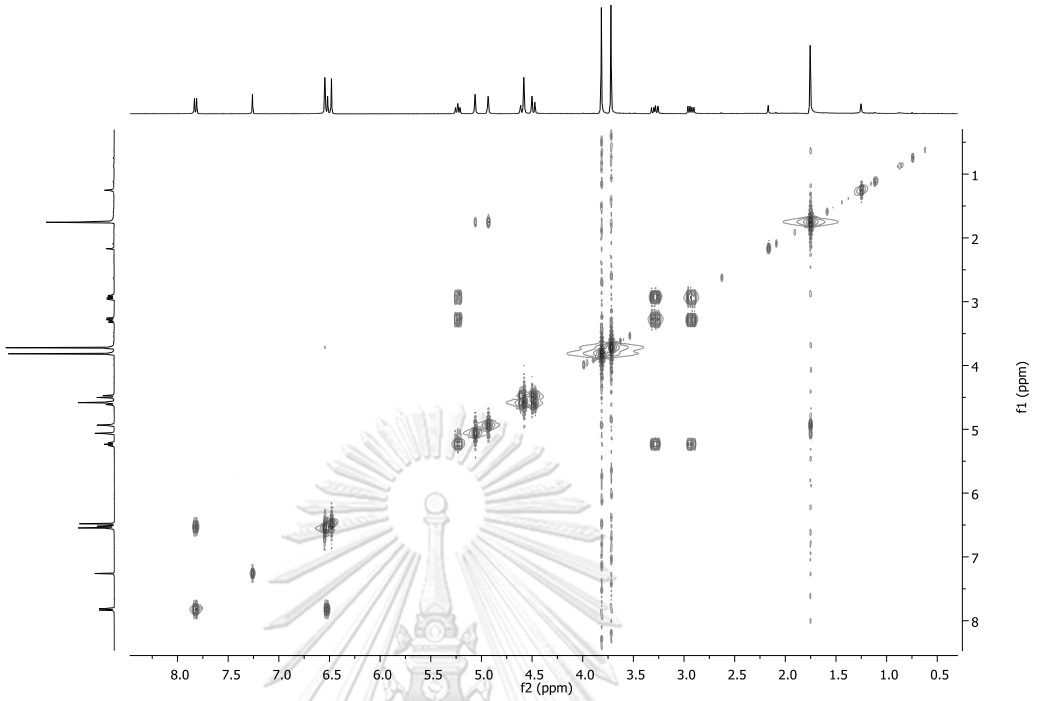

Figure A.19 ^{1}H-^{1}H COSY spectrum ($CDCl_3$) of compound **11**

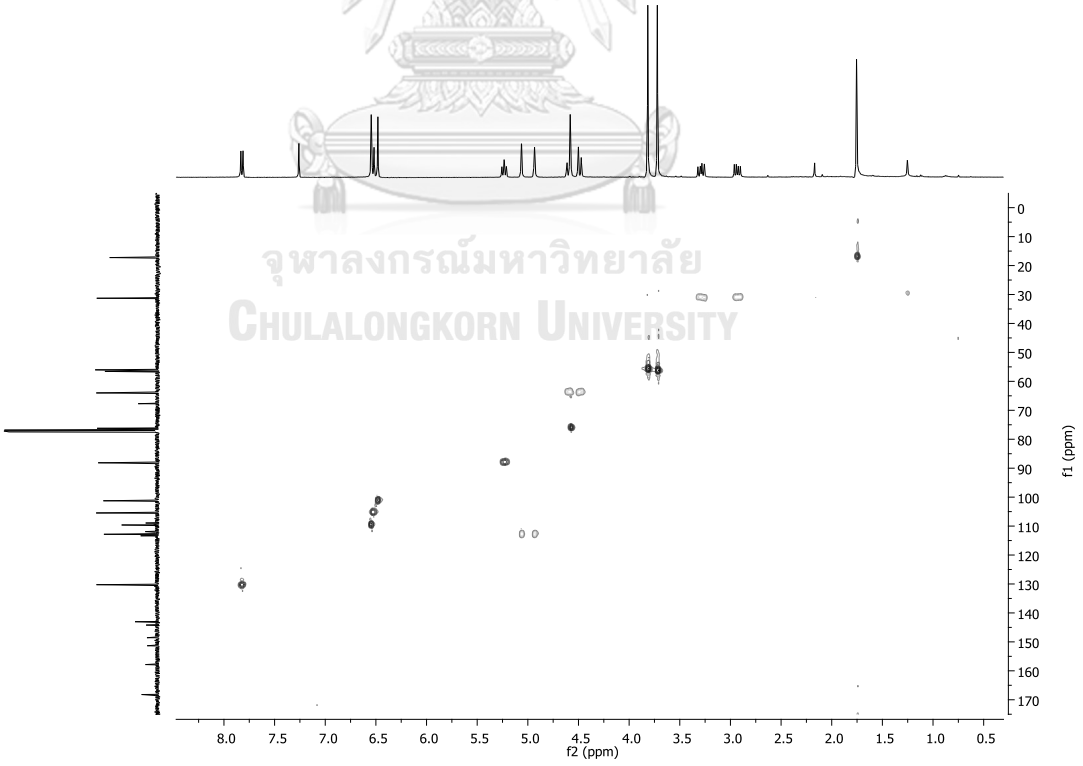

Figure A.20 HSQC spectrum ($CDCl_3$) of compound **11**

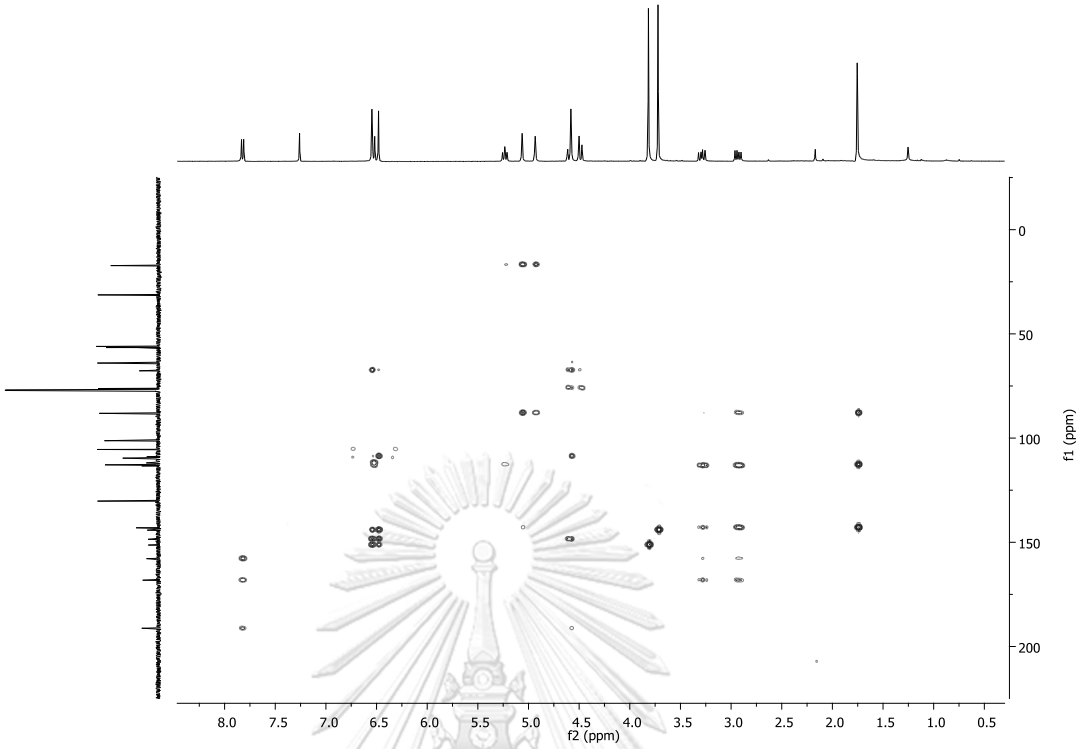

Figure A.21 HMBC spectrum ($CDCl_3$) of compound **11**

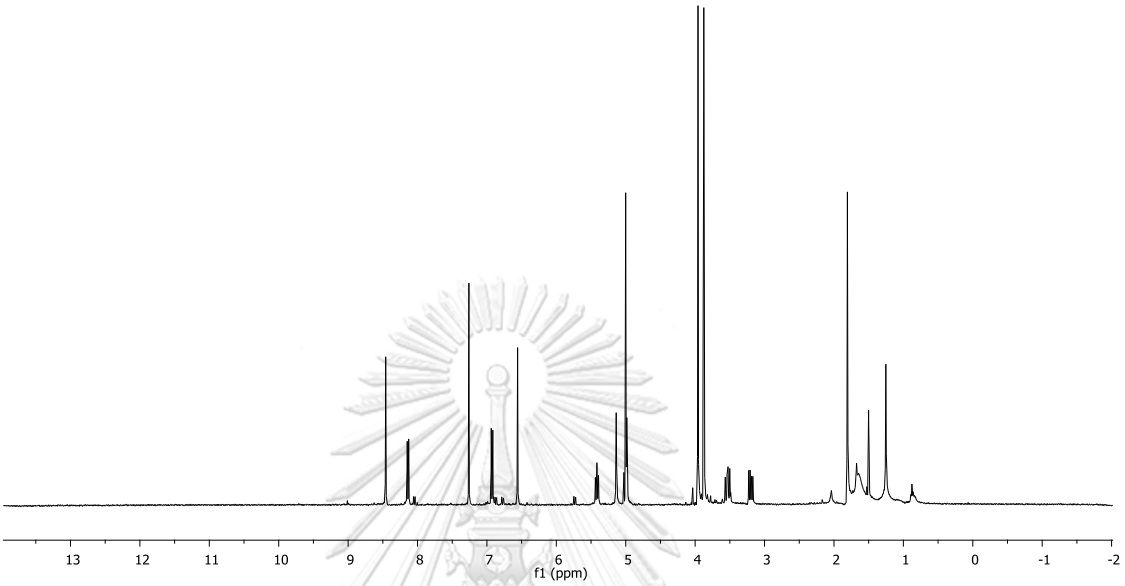

Figure A.22 ^{1}H NMR (400 MHz, $CDCl_3$) spectrum of compound **12**

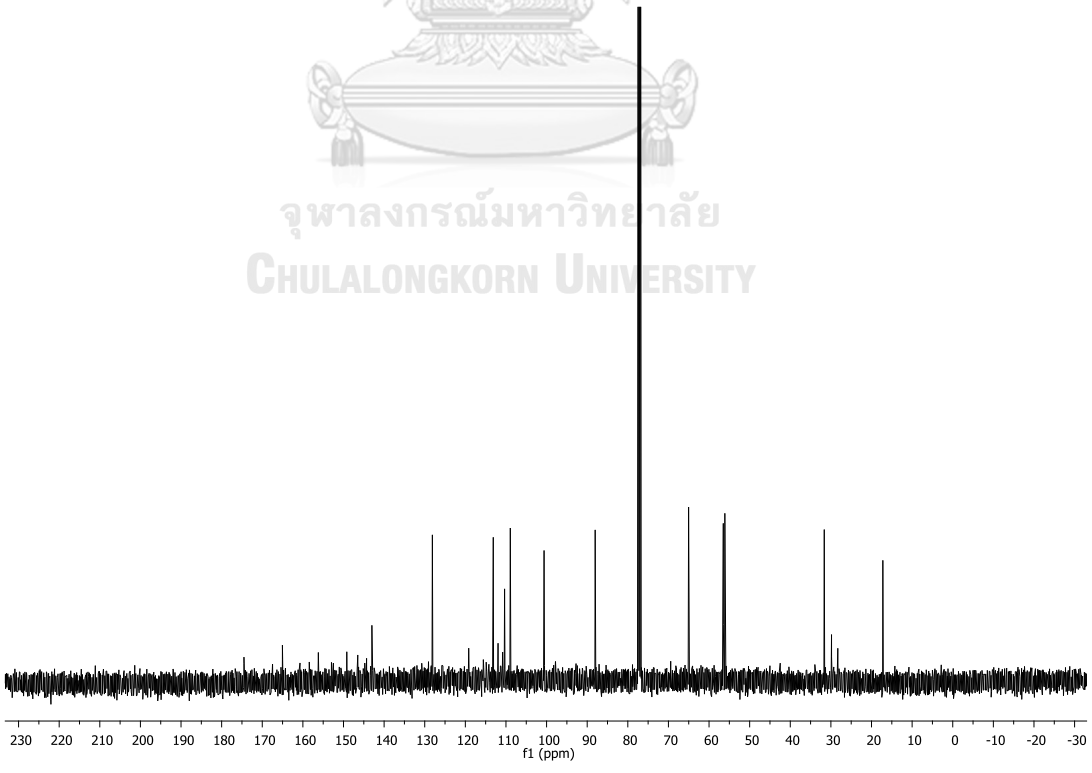

Figure A.23 ^{13}C NMR (100 MHz, $CDCl_3$) spectrum of compound **12**

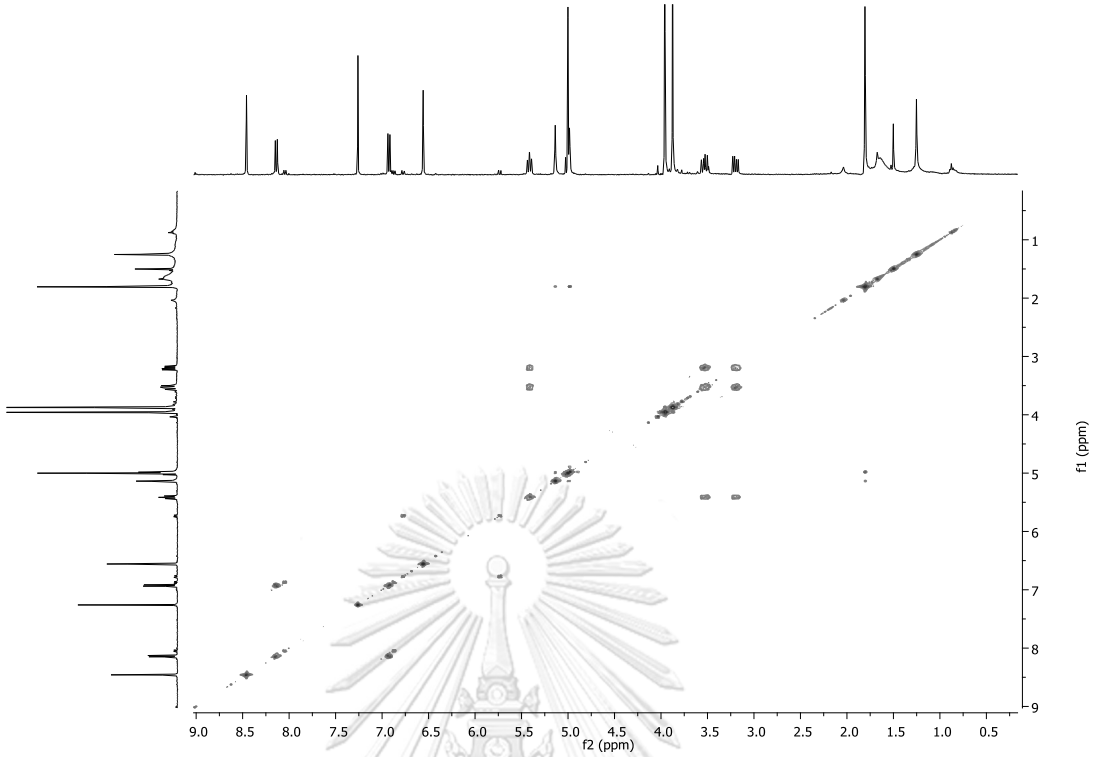

Figure A.24 ^{1}H-^{1}H COSY spectrum ($CDCl_3$) of compound **12**

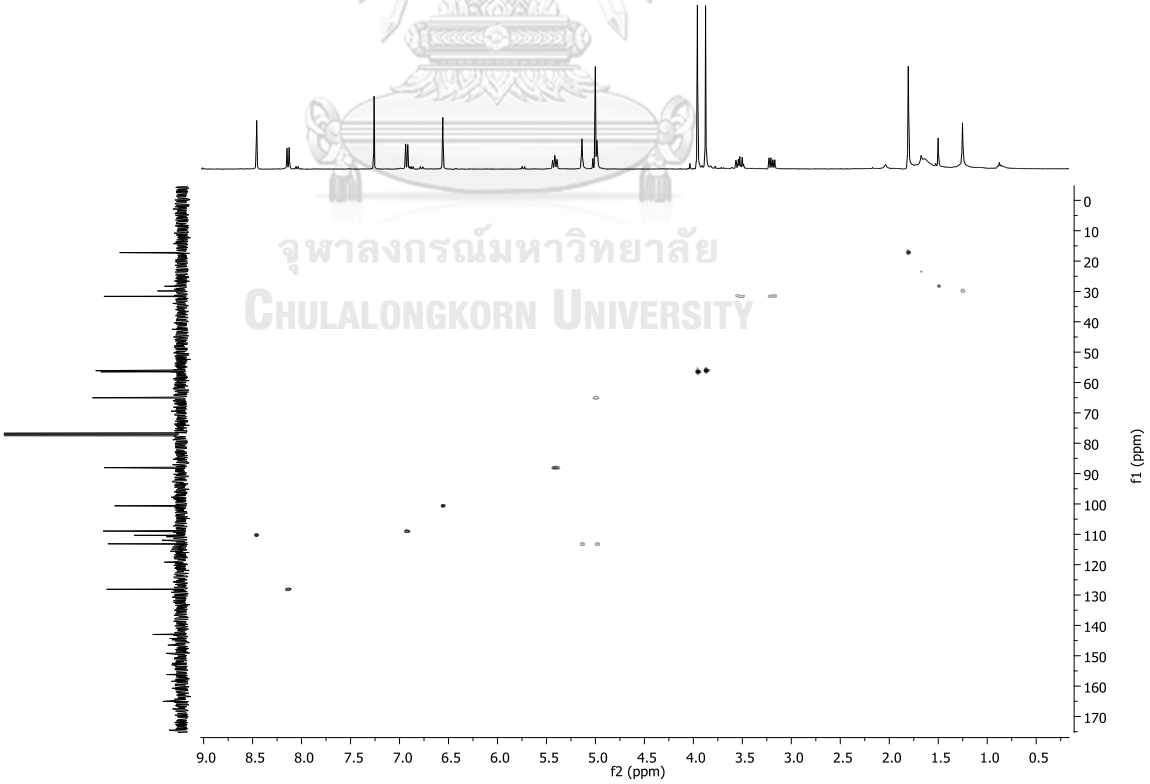

Figure A.25 HSQC spectrum ($CDCl_3$) of compound **12**

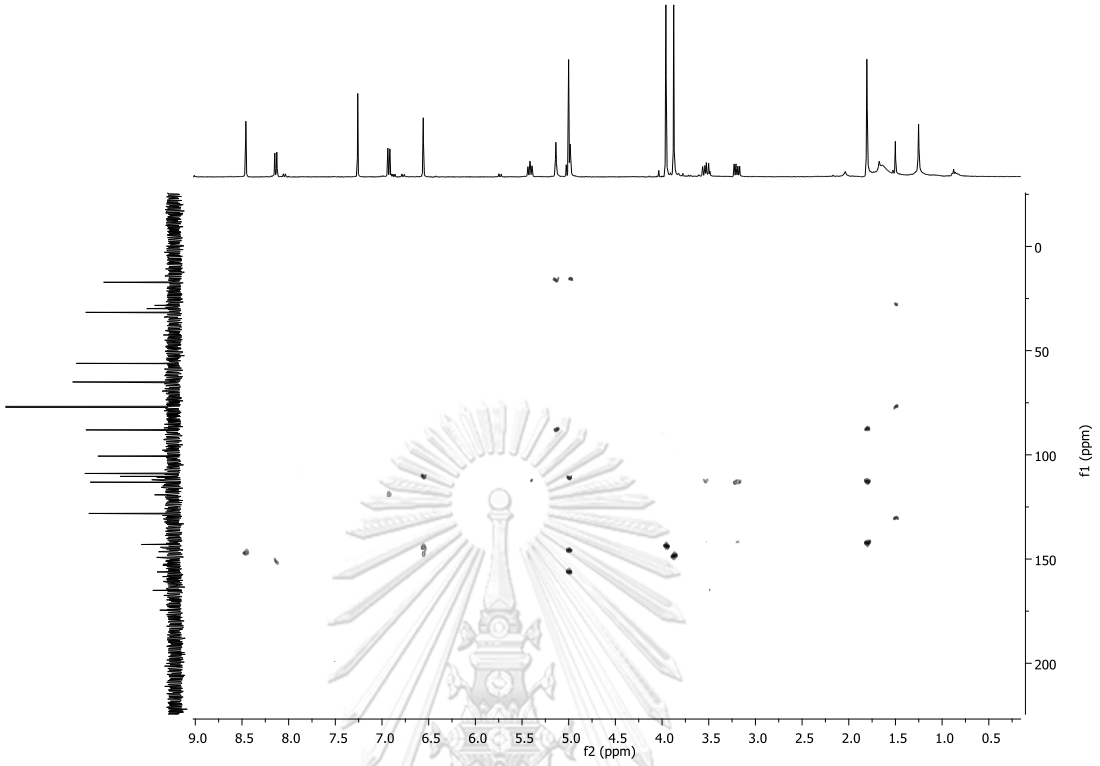

Figure A.26 HMBC spectrum ($CDCl_3$) of compound **12**

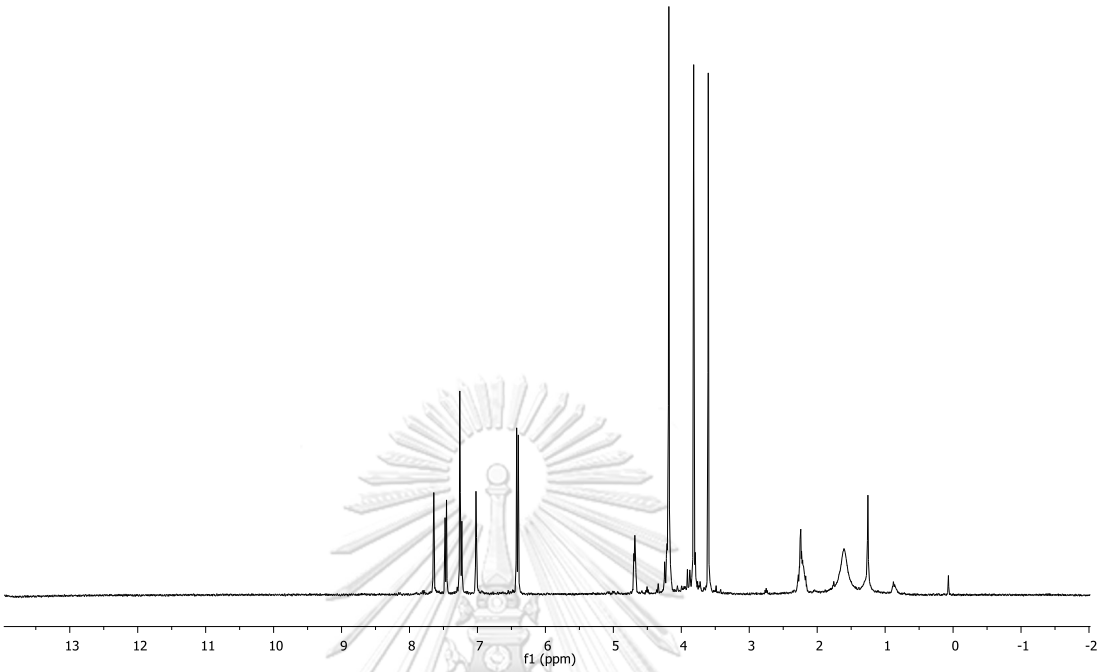

Figure A.27 ^{1}H NMR (400 MHz, $CDCl_3$) spectrum of compound **15**

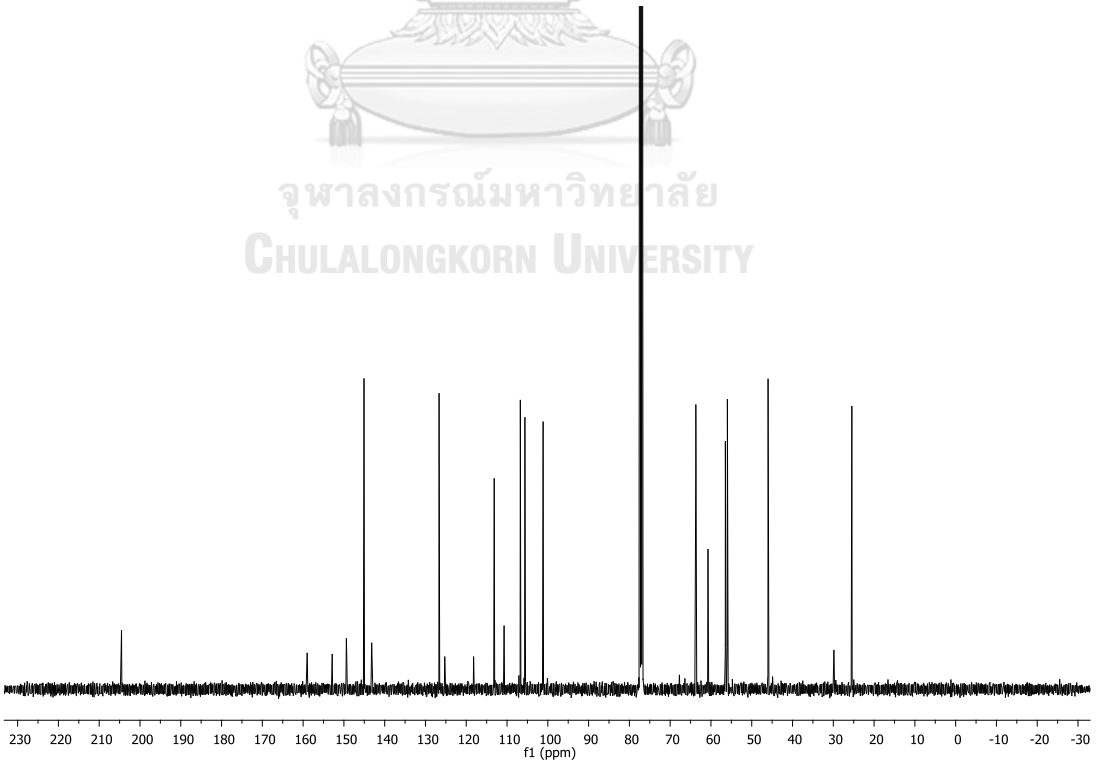

Figure A.28 ^{13}C NMR (100 MHz, $CDCl_3$) spectrum of compound **15**

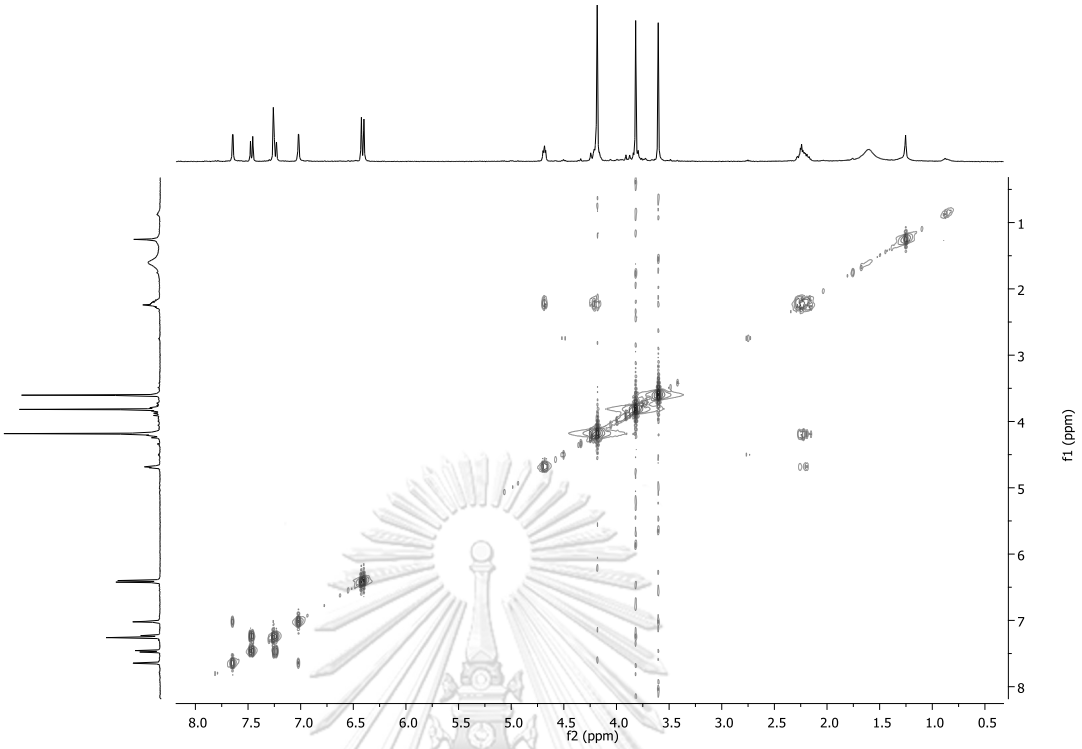

Figure A.29 ^{1}H-^{1}H COSY spectrum ($CDCl_3$) of compound **15**

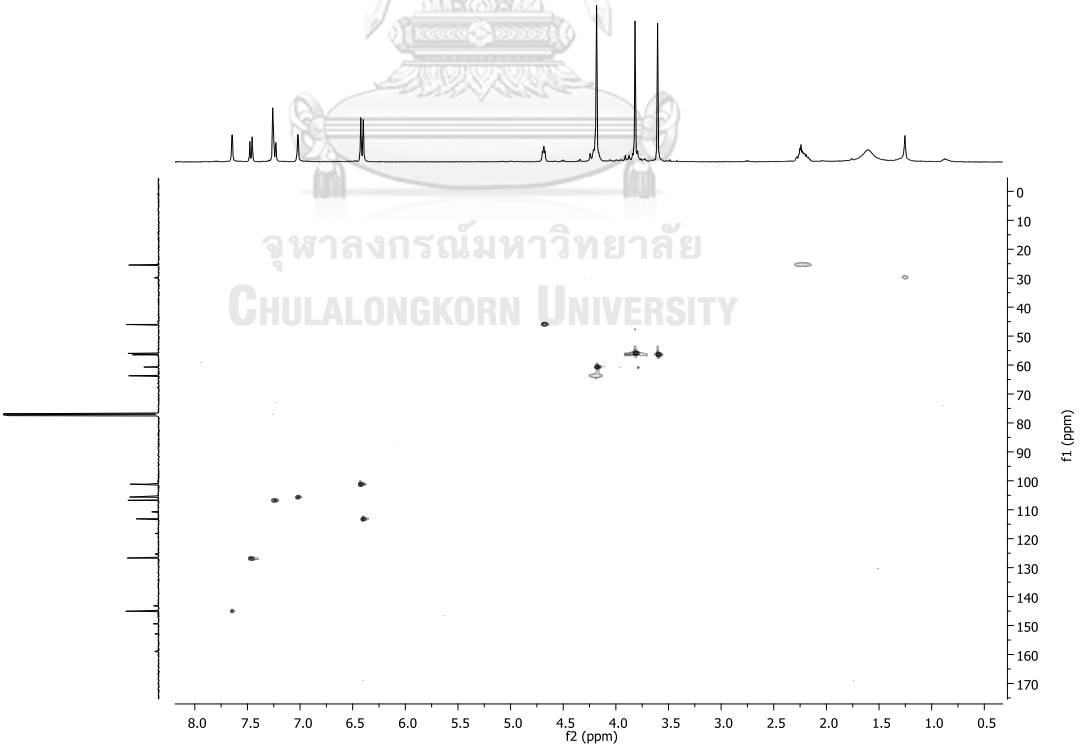

Figure A.30 HSQC spectrum ($CDCl_3$) of compound **15**

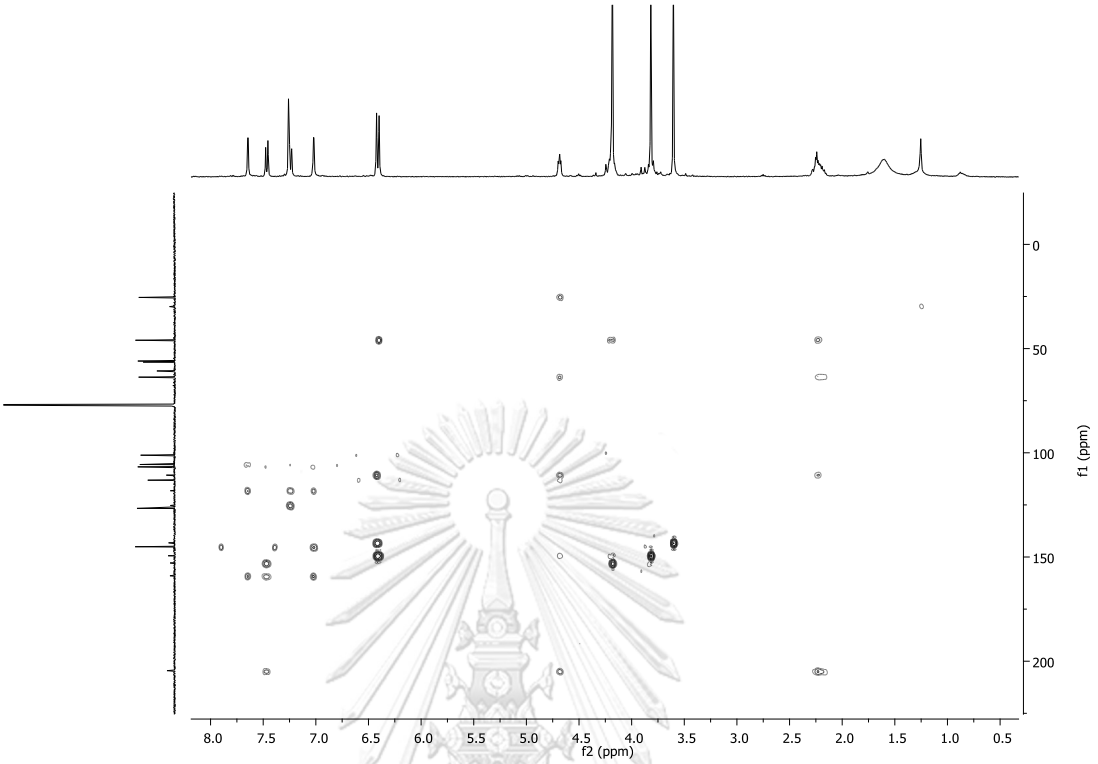

Figure A.31 HMBC spectrum ($CDCl_3$) of compound **15**

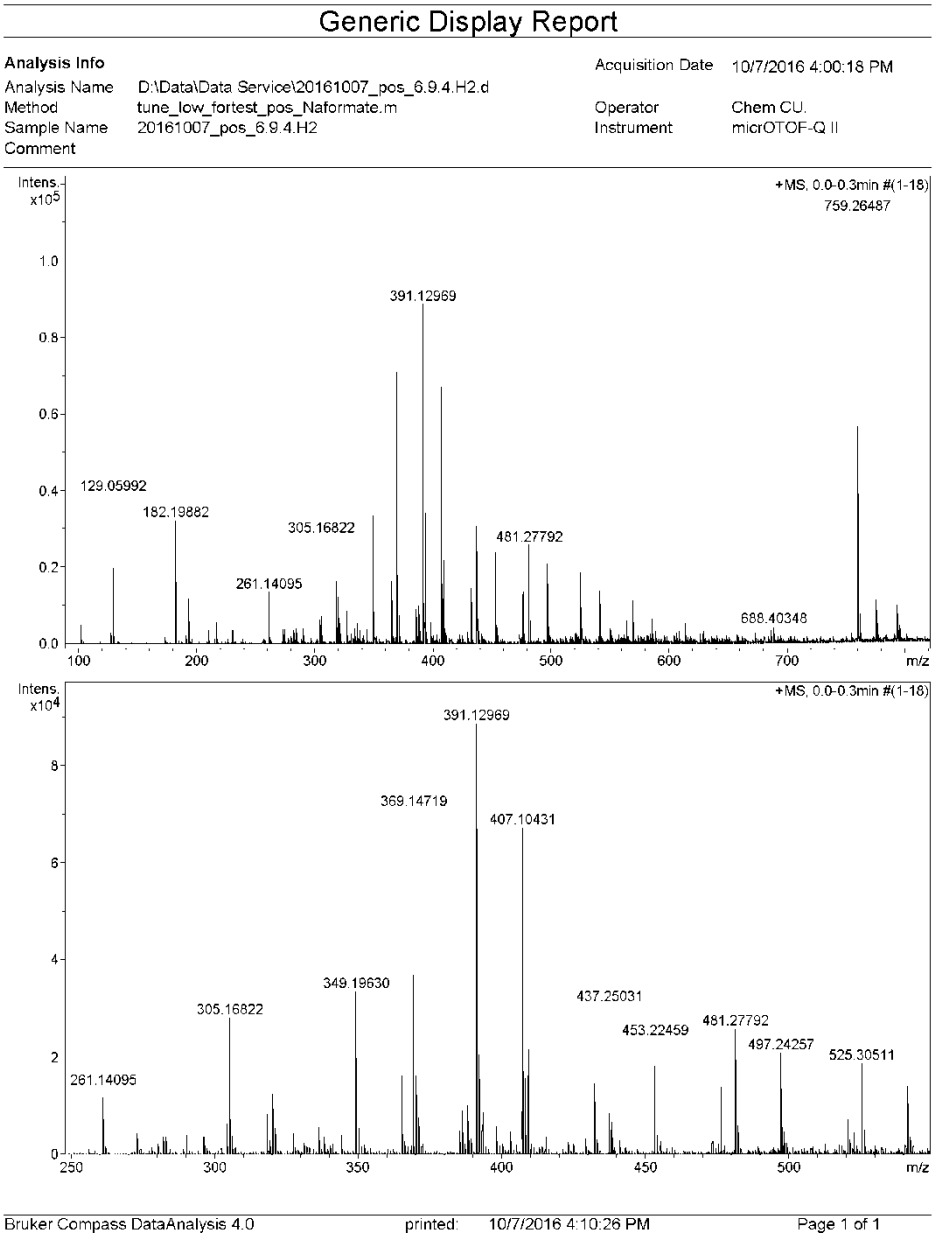

Figure A.32 HRESIMS Mass spectrum of compound **15**

VITA

Ms. Yanisa Mittraphab was born on November 22nd, 1991 in Chumphon, Thailand. She graduated with Bachelor's Degree in Science in Department of Chemistry from Faculty of Science, Chulalongkorn University, in 2013. During the time she was studied in the Master Degree in Department of Chemistry from Faculty of Science, Chulalongkorn University. She received the Overseas Research Experience Scholarship for Graduate Student for supporting her research project.

Her present address is 128/1 Village No. 11, Paramintaramankha 10 Rd. Bangmak Sub-district, Muang District, Chumphon, Thailand, 86000, Tel: +668-9731-4231.